Bonding Motifs of Noble-Gas Compounds as Described by the Local Electron Energy Density

Stefano Borocci, Maria Giordani, and Felice Grandinetti*

Dipartimento per la Innovazione nei sistemi Biologici, Agroalimentari e Forestali (DIBAF), Università della Tuscia, L.go dell'Università, s.n.c., 01100 Viterbo (Italy), and Istituto per le Metodologie Chimiche del CNR, Via Salaria, Km 29.500, 00015, Monterotondo, RM (Italy)

ABSTRACT

The bonding situation of some exemplary noble-gas (Ng) compounds, including HNg^+, HNgF, $FNgO^-$, Ng-HF, and NgBeO (Ng = He-Xe) was assayed by examining their local electron energy density $H(\boldsymbol{r})$. In general, this function partitions the space of atomic species (neutral and ionic) into inner regions of negative values, and outer regions of positive values. In the formation of chemical bonds, these atomic regions combine so to form a molecular $H(\boldsymbol{r})$, $H_{mol}(\boldsymbol{r})$, whose plotted form naturally shows the "covalent" and "non-covalent" regions of the molecular species, and allows also to recognize different types of non-covalent interactions such van der Waals, hydrogen, and ionic or partially ionic bonds. The qualitative assignment of the various bonding motifs is corroborated by the topological analysis of the $H_{mol}(\boldsymbol{r})$, which typically includes several critical points of rank 3 and variable signature. These points are, in particular, characterized here in terms of their bond degree (BD). Borrowing a previous definition (Espinosa et al. *J. Chem. Phys.* **2002**, *117*, 5529-5542), this quantity is taken as the ratio between the energy density calculated at the critical point of $H(\boldsymbol{r})$, $H(\boldsymbol{r}_c)$, and the corresponding electron density $\rho(\boldsymbol{r}_c)$: BD = $-H(\boldsymbol{r}_c)/\rho(\boldsymbol{r}_c)$. Thus, the BD is positive for covalent interactions [$H(\boldsymbol{r}_c) < 0$], and negative for non-covalent ones [$H(\boldsymbol{r}_c) > 0$]. For structurally-related species, the BD resulted, in general, positively correlated with the binding energies, and is, therefore, a semi-quantitative index of stability. The present study suggests the general validity of the $H_{mol}(\boldsymbol{r})$ to effectively assay the bonding motifs of noble-gas compounds.

Keywords: AIM Theory - Chemical Bonding - Local Electron Energy Density - Noble Gas Compounds - Theoretical Calculations

INTRODUCTION

The chemical inertness of the noble gases (Ng), and their general reluctance to form isolable compounds essentially reflect the resistance of the Ng atoms to form strong covalent bonds. Thus, only xenon and, partly, krypton have a rich bulk-phase chemistry, accessible under ordinary or nearly-ordinary conditions.[1-3] The stabilization of HArF, the only known argon compound, demands, instead, an ultra-cold environment,[4] and strongly-bound ions of helium and neon are detected only under the isolated conditions of the gas phase.[5] The difficulty to form covalent bonds does not mean, however, that the Ng atoms are truly hardest non-deformable spheres, crushable only under extreme conditions. Rather, the noble gases, including helium and neon, interact with neutral and ionic partners so to form bound species which range from weakest van der Waals adducts to more stable complexes with covalent contributions.[6-13] Thus, the tendency of the group 18 elements to maintain their closed-shell structure actually results in a richness of bonding motifs, which is, probably, unique in the periodic system. Over the years, this bonding versatility was continuously assayed by various theoretical methods, including, in particular, the topological analysis of the Electron Localization Function (ELF)[14-20], and of the electron density, the latter being performed within the Bader's theory of Atoms in Molecules (AIM).[21] Following pioneering applications reported so far,[22-25] the AIM theory is extensively employed to analyze the bonding situation of noble-gas compounds.[26-31] In general, within the AIM theory, one explores the topology of the electron density $\rho(\boldsymbol{r})$, and calculates the value of $\rho(\boldsymbol{r})$ and its Laplacian $\nabla^2\rho(\boldsymbol{r})$ at the (3,-1) critical points [$\nabla\rho(\boldsymbol{r}) = 0$] located on the gradient paths connecting the various bonded atoms (bond critical points, BCPs). Thus, for typical covalent bonds, at the BCP

$\rho(\boldsymbol{r})$ is relatively large and $\nabla^2\rho(\boldsymbol{r}) < 0$, while for typical non-covalent (closed-shell) interactions such as ionic bonds, hydrogen bonds, and van der Waals contacts, at the BCP $\rho(\boldsymbol{r})$ is relatively small, and $\nabla^2\rho(\boldsymbol{r}) > 0$.[21] These criteria, however, must often contend with conflicting indications from independent evidence, and further analysis is required. In particular, Cremer and Kraka[32,33] suggested so far to relate the covalent character of a bond with the sign of the local energy density $H(\boldsymbol{r})$ at the corresponding BCP, $H(\boldsymbol{r})$ being the sum of the local electron kinetic energy density $G(\boldsymbol{r})$ (the so-called Lagrangian electron kinetic energy density), and the local electron potential energy density $V(\boldsymbol{r})$. Thus, if at the BCP $\nabla^2\rho(\boldsymbol{r}) > 0$ but $H(\boldsymbol{r}) < 0$, the interaction is covalent or, at least, it possesses some degree of covalency. Complementary conditions such as $-G(\boldsymbol{r})/V(\boldsymbol{r}) < 0.5$ and $G(\boldsymbol{r})/\rho(\boldsymbol{r}) < 1$ were also derived.[21,34] Thus, in the AIM practice, the energy density $H(\boldsymbol{r})$ is typically employed as a "point" index, used to catch, through the sign of $H(\boldsymbol{r})$ at the BCP, bonding contributions which escape to other indices. In particular, pursuing along this direction, a general classification of the interactions occurring in noble-gas compounds was recently proposed.[35]

In a very recent study,[36] we found that the bonding situation of the complexes of $XeHXe^+$ with simple ligands, invariably described by various methods of bonding analysis as weakly-bound, non-covalent adducts, could be also successfully caught by examining the plotted form of their $H(\boldsymbol{r})$ function [or, equivalently, of its opposite $K(\boldsymbol{r})$, the so-called Hamiltonian electron kinetic energy density]. In the present study, we show that the full analysis of $H(\boldsymbol{r})$ is, indeed, a general tool to effectively assay the bonding motifs of noble-gas compounds. The qualitative character of the various interactions naturally emerges from the plotted form of $H(\boldsymbol{r})$, and the examination of the

topology of this function furnishes also semi-quantitative indications on their relative extent.

The paper is organized as follows. In the first part, we discuss the $H(\boldsymbol{r})$ functions of some atomic species, and show how they generally combine so to sign the bonding situation of some exemplary non-covalent, covalent, and ionic species. In the second part, we discuss the $H(\boldsymbol{r})$ of some exemplary noble-gas compounds, and the description of their bonding motifs furnished by this function.

COMPUTATIONAL DETAILS

The theoretical level employed in this study was the coupled cluster with inclusion of single and double substitutions, CCSD, and an estimate of connected triples, CCSD(T),[37] used in conjunction with the Dunning's correlation consistent triple-zeta basis set (aug-cc-pVTZ).[38-42] The Xe atom was treated by the Stuttgart/Cologne small-core (28 electrons), scalar-relativistic effective core potential (ECP-28),[43] and the jointly-designed (13*s*12*p*10*d*2*f*)/[6*s*5*p*4*d*2*f*] aug-cc-pVTZ-PP basis set.[43] The energy density and the electron density were calculated at the CCSD/aug-cc-pVTZ level of theory, and analyzed with the Multiwfn program (version 3.6.6)[44] using the wfn or wfx input files generated by the Gaussian 03[45] or the Gaussian 09[46] (in the CCSD calculations, the convergence criteria were 10^{-8} hartree on the energy and 10^{-6} on the change in the cluster amplitudes). The values of $H(\boldsymbol{r})$ and $\rho(\boldsymbol{r})$ are expressed in atomic units [for $\rho(\boldsymbol{r})$, 1 au = 1 e a_0^{-3} = 6.7483 e Å^{-3}; for $H(\boldsymbol{r})$, 1 au = 1 hartree a_0^{-3} = 6.7483 hartree Å^{-3}]. The CCSD/aug-cc-pVTZ $H(\boldsymbol{r})$ and $\rho(\boldsymbol{r})$ were, in particular, calculated at the CCSD(T)/aug-cc-pVTZ optimized geometries obtained in the present study (Ng-HF,

Kr_2, Xe_2) or taken from the literature [H_2,[47] HF,[47] F_2,[47] NaF,[47] NaCl,[47] BeO,[47] Ng_2 (Ng = He-Ar[48,49]), NgH^+,[50] $FNgO^-$,[51,52] NgBeO,[53] and HNgF[53]]. The two- (2D) plots of $H(\boldsymbol{r})$, and three-dimensional (3D) plots of the critical points located from its topological analysis were as well obtained using the Multiwfn. In particular, the 2D plots include the contour lines belonging to the patterns $\pm k \times 10^n$ (k = 1, 2, 4, 8; n = -4 ÷ 6), and the contour lines corresponding to the critical points of $H(\boldsymbol{r})$.

RESULTS AND DISCUSSION

A. The $H(\boldsymbol{r})$ of Atomic Species. In general, the $H(\boldsymbol{r})$ function partitions the space of atomic species (neutral and ionic) into an inner region of negative values, henceforth indicated as $H^-(\boldsymbol{r})$, and an outer region of positive values, henceforth indicated as $H^+(\boldsymbol{r})$. Subfigures a-f of Figures 1 and 2 show the $H(\boldsymbol{r})$ of some exemplary species, including the Ng atoms.

<Figures 1 and 2 near here, please>

In the $H^-(\boldsymbol{r})$ region, the function is minimum at the nucleus, and progressively decreases up to zero. This decrease is monotonic, for example, for H, He, and Kr, but, in general, it passes through local minima and maxima, which sometimes reflect the existence of inner tiny $H^+(\boldsymbol{r})$ region(s) enclosed between two $H^-(\boldsymbol{r})$ sub-regions. This happens, for example, for the isoelectronic Ar (Figure 1d) and Cl^- (Figure 2d). For the open-shell species, the position and height of the local minima and maxima depend on the direction, and this produces, in planes containing orbitals of different occupancies, non-spherical contour lines that visually sign the orbitals itself. In particular, doubly-occupied orbitals appear as two lobed regions of negative contour lines, and singly-

occupied or empty orbitals appear as two lobed regions of positive values enclosed between lobed contour lines of negative values. For example, the contour lines of F (assumed here to be $1s^2 2s^2 2p_x^2 2p_y^2 2p_z$) are spherically symmetric in the *xy* plane (Figure 2a), but asymmetric in the two equivalent *xz* or *yz* planes (Figure 2b). The local minima and maxima of F fall, in particular, close to the nucleus (between ca. 0.15 Å and ca. 0.25 Å), and the differences in the contour lines corresponding to the two orbitals of different occupancies are visualized in this region. Also, we note from Figures 1 and 2 that the size of the $H^-(\boldsymbol{r})$ regions of the various atomic species follow certain regularities, which mirror typical trends of atomic and ionic size. For example, the size of the $H^-(\boldsymbol{r})$ region of the Ng atoms progressively increases from He (0.590 Å) to Xe (1.597 Å), the size of the $H^-(\boldsymbol{r})$ region of F^- (0.950 Å) is slightly larger than that of F (0.910 Å) but significantly smaller than that of Cl^- (1.442 Å), and the size of the $H^-(\boldsymbol{r})$ region of Li^+ (0.389 Å) is smaller than that of Na^+ (0.638 Å).

In the outer $H^+(\boldsymbol{r})$ region, $H(\boldsymbol{r})$ becomes vanishingly small at the largest distances, typically passing through a point of maximum. Figure 3a shows, for example, the radial dependence of the $H(\boldsymbol{r})$ of He in the outer region. The corresponding graphs of the other Ng atoms are qualitatively similar, the height of the maximum following the irregular periodic trend Ne (0.01219 hartree a_0^{-3}) > He (0.00507 hartree a_0^{-3}) > Ar (0.00188 hartree a_0^{-3}) > Kr (0.00100 hartree a_0^{-3}) > Xe (0.00053 hartree a_0^{-3}). For some atomic species, the outer $H^+(\boldsymbol{r})$ region may include additional maxima of lower eight. Figure 3b shows the exemplary case of F^-.

<Figure 3 near here, please>

B. The Molecular $H(\boldsymbol{r})$ as an Indicator of Chemical Bonding. In the formation of chemical bonds, the atoms combine their $H^-(\boldsymbol{r})$ and $H^+(\boldsymbol{r})$ regions so to form a molecular

$H_{mol}(\boldsymbol{r})$. We first discuss how this function signs the bonding situation of some prototypical non-covalent, covalent, and ionic species.

In general, the character of the various interactions is assigned by visual inspection of the plotted form of $H_{mol}(\boldsymbol{r})$, and by examination of its topology. The latter typically includes various critical points [namely, space points where $\nabla H_{mol}(\boldsymbol{r}) = 0$], henceforth indicated as HCPs, of rank $\hat{r} = 3$, and signature s = -3, -1, +1, or +3 [at any HCP, $\hat{r}$ is the rank of the matrix given by the number of nonzero eigenvalues of the Hessian matrix of $H_{mol}(\boldsymbol{r})$, and s is the summation of their signing numbers, conventionally assigned as -1 to a negative eigenvalue, and as +1 to a positive eigenvalue]. In particular, the study of numerous neutral and ionic molecular species furnished the following general indications:

1) in the formation of a chemical bond A-B, the involved atoms overlap contour lines of the same value [henceforth indicated as $H(\boldsymbol{r})$ isolines]. A and B never overlap contour lines of opposite sign;
2) in typical non-covalent interactions (e.g. van der Waals or hydrogen bonds), A and B overlap some isolines of their outer $H^{+}(\boldsymbol{r})$ regions. In the simplest cases, this process, henceforth indicated as H^{+}(A)-H^{+}(B), is signed by a single (3,-1) HCP along the bond axis (henceforth assumed to be z). At this critical point, $H_{mol}(\boldsymbol{r})$ is, in fact, minimum along z (s = +1), and maximum along the two perpendicular directions x and y (s = -1). Other topologies are more complex, and typically include HCPs of different type falling off axis. For species of axial symmetry, the latter appear as ring(s) of degenerate HCPs;
3) in typical covalent bonds, A and B overlap all the positive isolines of their outer $H^{+}(\boldsymbol{r})$ regions, as well as some negative isolines of their inner $H^{-}(\boldsymbol{r})$ regions. The

latter process, henceforth indicated as H^-(A)-H^-(B), is generally signed by a single (3,+1) HCP falling on the bond axis. At this critical point, $H_{mol}(\boldsymbol{r})$ is, in fact, maximum along z (s = -1) and minimum along x and y (s = +1);

4) in a typical ionic bond A^+B^-, the atom B overlaps all (or nearly all) the contour lines of its outer $H^+(\boldsymbol{r})$ region with some isolines of the outer $H^+(\boldsymbol{r})$ region of A. This H^+(A)-H^+(B) interaction, typically signed by HCPs falling off axis, brings the inner $H^-(\boldsymbol{r})$ region of B in close contact with the outer $H^+(\boldsymbol{r})$ region of A, and visually appears as the proximity of these two zones, generally mutually polarized. As a matter of fact, this proximity of polarized $H(\boldsymbol{r})$ regions of opposite sign distinguishes ionic bonds (or bonds with ionic contributions) from other types of closed-shell interactions.

Some exemplary cases of non-covalent, covalent, and ionic bonds are discussed below.

The Ng_2 complexes (Ng = He-Xe) are exemplary cases of non-covalent interactions. Their bonding situation is clearly caught by inspecting subfigures a-e of Figure 4, which show the $H_{mol}(\boldsymbol{r})$ plotted in the main molecular plane. The Ng atoms undergo a H^+(Ng)-H^+(Ng) interaction, leaving their $H^-(\boldsymbol{r})$ regions well separated and, essentially, unperturbed (see also Figure 1 for comparison). For Ng = He, Ar, Kr, and Xe, this produces a single (3,-1) HCP falling at the center of the bond axis. For Ne_2, the central zone actually includes three quite close HCPs, namely a pair of degenerate (3,-1), separated by a (3,-3). The values of the energy density $H(\boldsymbol{r}_c)$, and of the electron density $\rho(\boldsymbol{r}_c)$ calculated at the central HCPs of the Ng_2 are listed in Table 1.

<Figure 4 and Table 1 near here, please>

In 2002, Espinosa et al.[54] introduced the bond degree (BD) as the ratio between the energy density calculated at the BCP predicted from the topological analysis of $\rho(\boldsymbol{r})$,

and the corresponding electron density. In particular, for non-covalent interactions, this ratio was taken as a measure of softening degree (SD): the weaker the interaction, the greater the magnitude of SD. In the present study, we borrow the concept of BD, and, irrespective of the interaction type, we take it as the minus of the ratio between the energy density calculated at the HCP, $H(\boldsymbol{r}_c)$, and the corresponding electron density $\rho(\boldsymbol{r}_c)$: BD = $-H(\boldsymbol{r}_c)/\rho(\boldsymbol{r}_c)$. Thus, BD is positive for covalent interactions [$H(\boldsymbol{r}_c) < 0$], and negative for non-covalent ones [$H(\boldsymbol{r}_c) > 0$]. One also expects that, for covalent bonds, the stronger the interaction, the higher the BD. Conversely, for non-covalent bonds, the weaker the interaction, the lower (more negative) the BD. A first confirmation of these expectations comes from the data quoted in Table 1. We note, in particular, a positive correlation between the CCSD(T)/aug-cc-pVTZ electronic binding energies ΔE of the Ng_2, progressively increasing from He_2 (0.02 kcal mol^{-1}) to Xe_2 (0.82 kcal mol^{-1}), and the BD, progressively increasing in the same order from -0.463 hartree e^{-1} to -0.180 hartree e^{-1}. In their investigation, Espinosa et al.[54] found also that, for a series of pure closed-shell neutral complexes XH···FY, the H···F interaction energies were linearly correlated with the SD. As for complexes involving atoms of different type, such linear correlations are, in general, not expected, and, in fact, the dependence on BD of the ΔE of the Ng_2 is not linear ($r^2 = 0.686$). The data are, instead, reasonably well fitted by an exponential function ($r^2 = 0.941$), and similar dependencies were also obtained for other groups of investigated compounds (*vide infra*). In presenting such dependencies we note, however, the intrinsic limitations of any direct correlation between ΔE and BD. The ΔE, in fact, strongly depends on the density relaxation mechanism of the fragments,[55] and even for the slightly polarized Ng_2, the relaxation energies are different because of different numbers of core shells and effective atomic numbers. In addition, a

single density value at a HCP hardly reflects the intrinsic ΔE, which is better related to the whole density in the bond region.

A closer inspection of subfigures a-e of Figure 4 reveals that some contour lines of the positive regions are non-spherical, and that this effect becomes progressively more pronounced passing from He_2 to Xe_2. We could ascertain that these asymmetries actually reflect the mutual effect of the two Ng atoms, which affect the contour lines according to the following mechanism. In the $H^+(\boldsymbol{r})$ region of any Ng (see Figure 3a for He), due to the presence of the point of maximum, any value of $H(\boldsymbol{r})$ (with the exception of the maximum itself) actually corresponds to a pair of spherical degenerate contour lines, which fall at different distances from the nucleus. In the presence of the second Ng atom, these isolines are polarized toward the center of the Ng_2. However, the ensuing distortion is different for the two lines, and, for certain values of $H(\boldsymbol{r})$, the two differentially-distorted isolines come in contact, and, in the touching zone(s), they simply disappear. This partially destructive interference produces HCPs which typically fall off the bond axis. Due to axial symmetry, in the 3D view of the topology of the $H_{mol}(\boldsymbol{r})$ (see subfigures f-l of Figure 4), these HCPs appear as distorted planes (He_2), or rings lying in planes perpendicular to the bond axis (Ne_2-Xe_2).

Figure 5 shows the $H_{mol}(\boldsymbol{r})$ of H_2, HF, and F_2 plotted in the main molecular plane (subfigures a-c). The covalent character of these species is visually caught as the overlap of the $H^-(\boldsymbol{r})$ regions of the involved atoms, and topologically signed by a (3,+1) critical point falling at the centre (H_2 and F_2) or near the centre (HF) of the molecule. The properties of these covalent HCPs are listed in Table 2.

<Figure 5 and Table 2 near here, please>

As expected, the corresponding values of the BD are definitely positive, and, interestingly, they increase in the same order of the homolytic bond dissociation energies, namely $F_2 < H_2 < HF$. Besides the covalent HCPs, the topology of the $H_{mol}(\boldsymbol{r})$, shown in subfigures d-f of Figure 5 includes, in particular, rings of degenerate HCPs lying in planes perpendicular to the bond axis. For H_2, these critical points arise exclusively from the non-covalent H^+(H)-H^+(H) interaction which preludes the formation of the covalent bond. For HF and F_2, the ring(s) surrounding the F atom(s) are, instead, the signature of the lone-pairs, visualized also by featuring contour lines in the planar plots of Figure 5b and 5c (see also Figure 2b for comparison). For the symmetric H_2 and F_2, both the (3,+1) HCP and the (3,-1) BCP predicted from the topological analysis of $\rho(\boldsymbol{r})$ fall, as expected, at the center of the molecule. However, for the asymmetric HF, the BCP falls at 0.14 Å from H, but the corresponding distance of the HCP is 0.31 Å. Interestingly, the latter value is nearly coincident with the covalent radius of H (0.32 Å[56]).

Subfigures a and b of Figure 6 show the $H_{mol}(\boldsymbol{r})$ of NaF and NaCl plotted in the main molecular planes.

<Figure 6 near here, please>

These ionic species (the CCSD/aug-cc-pVTZ NBO atomic charges amount, respectively, to ± 0.950 *e* and ± 0.921 *e*) undergo a H^+(Na)-H^+(X) interaction (X = F, Cl), which is signed by pairs of degenerate HCPs, placed symmetrically with respect to the bond axis, and belonging to ring structures perpendicular to *z*. The X atom overlaps most of the contour lines of its outer $H^+(\boldsymbol{r})$ region, and this brings its inner $H^-(\boldsymbol{r})$ region in close proximity of the outer $H^+(\boldsymbol{r})$ region of Na. This H^+(Na)-H^-(X) close contact is, indeed, the main signature of the ionic character of the bond, visually-caught as the

mutual polarization of the contour lines of the involved atoms (the ensuing electrostatic interaction does not produce any HCP along the bond axis). The effect is particularly evident for X, whose $H^-(\boldsymbol{r})$ region (particularly the outest contour lines) is distorted into non-spherical envelopes of featuring shapes. Interestingly, this distortion is more pronounced for the larger and more polarizable Cl. It is also worthmentioning that the BCP predicted from the topological analysis of $\rho(\boldsymbol{r})$ falls on a positive contour line which belongs to the $H^+(\boldsymbol{r})$ region of Na, and is in close proximity of the borderline between the $H^+(\boldsymbol{r})$ region of Na and $H^-(\boldsymbol{r})$ region of X [$H(\boldsymbol{r})$ = 0.01092 hartree a_0^{-3} for NaF and 0.00429 hartree a_0^{-3} for NaCl].

As shown in Figure 6c, for BeO the polarization of the $H^-(\boldsymbol{r})$ region of O arising from the H^+(Be)-H^-(O) interaction is so pronounced that its negative contour lines visually "embrace" the outer $H^+(\boldsymbol{r})$ region of Be, with an eventual encapsulation effect. As a matter of fact, for the higher negative values of $H(\boldsymbol{r})$, the contour lines of O interact with the polarized isolines of Be, and, at $H(\boldsymbol{r})$ = -3.7×10^{-5} hartree a_0^{-3}, this H^-(Be)-H^-(O) interaction is signed by a (3,-1) HCP with a positive BD of 0.123 hartree e^{-1} (see the dot of Figure 6c). Thus, based on the analysis of the $H_{mol}(\boldsymbol{r})$, BeO is assigned as an ionic species, with a contribution of covalency, or, alternatively, as a strongly-polarized covalent bond. As a matter of fact, the CCSD/aug-cc-pVTZ NBO atomic charges of BeO amount to ± 1.718 *e*. Interestingly, the BCP located on the Be-O bond path from the topological analysis of $\rho(\boldsymbol{r})$ is again at the borderline between the $H^+(\boldsymbol{r})$ region of Be and the $H^-(\boldsymbol{r})$ region of O, but, unlike NaF and NaCl, it falls on a $H(\boldsymbol{r})$ contour line of negative value (-0.04653 hartree a_0^{-3}). Thus, in the bonding analysis based on the $H_{mol}(\boldsymbol{r})$, the position of the BCP may distinguish between purely ionic (e.g. NaF and NaCl), and strongly-polarized covalent bonds.

C. Bonding Motifs of Noble-Gas Compounds. We turn now to discuss the bonding situation of some exemplary noble-gas compounds in terms of their $H_{mol}(\boldsymbol{r})$. The investigated species, including, in particular, HNg^+, HNgF, $FNgO^-$, Ng-HF, and Ng-BeO, were selected for their diverse bonding motifs, as well as for the widespread experimental and theoretical interest that they have attracted over the years.

HNg^+ and HNgF. The diatomic HNg^+ (Ng = He-Xe) are quite stable in the gas phase, and thoroughly investigated since long time.[5,57-62] Their bond distances and vibrational frequencies are known from spectroscopic measurements,[57-61] and numerous other molecular properties were already investigated by various theoretical methods (particularly for the heaviest congeners[62]). Interestingly, HAr^+ was recently detected in the Crab nebula[63] and in other interstellar regions,[64,65] and this opens exciting questions concerning the conceivable role of noble-gas molecular species in the chemistry of the interstellar medium. The neutral HNgF (Ng = He, Ar, Kr, Xe) are prototype examples among the family of noble-gas hydrides discovered over the last two decades by Räsänen and co-workers.[66-69] These HNgY (Ng = noble gas atom; Y = electronegative fragment) are obtained by photodissociation of HY in a cold Ng matrix, and are, in general, best described by the resonance form $(HNg^+)Y^-$. The observed HNgF include, in particular, HArF, a first (and to date unique) neutral argon compound,[4] and HKrF.[70] The predicted HXeF[71] is still waiting the experimental detection, while HHeF[72] is probably too short-lived to be trapped even at low temperature.[73] At the highest levels of theory, HNeF is, instead, intrinsically unstable.[72]

The covalent character of the HNg^+ (Ng = He-Xe) is clearly caught by inspecting subfigures a-e of Figure 7, which show the $H_{mol}(\boldsymbol{r})$ plotted in the main molecular plane.

The H^-(H)-H^-(Ng) interaction produces an inner "negative" region, with a (3,+1) HCP falling on the bond axis. The properties of these critical points are listed in Table 3.

<Figure 7 and Table 3 near here, please>

One first notes that these HCPs are invariably closer to the H atom, the r(H) distance progressively increasing passing from HHe^+ (0.287 Å) to HXe^+ (0.562 Å). This reflects an outer overlapped contour line, corresponding to $H(\boldsymbol{r}_c)$, of progressively lower value. Meanwhile, the electron density $\rho(\boldsymbol{r}_c)$ decreases from HHe^+ to HXe^+, the only irregularity being the value of HNe^+ (0.3085 $e\ a_0^{-3}$) slightly higher than that of HHe^+ (0.2716 $e\ a_0^{-3}$). In any case, passing from HHe^+ to HXe^+, the BD progressively decreases from 1.218 hartree e^{-1} to 0.840 hartree e^{-1}, and this suggests a periodical decrease of the strength of the H-Ng^+ covalent interaction.

The plotted $H_{mol}(\boldsymbol{r})$ of the neutral HNgF (Ng = He, Ar, Kr, Xe), shown in subfigures f-i of Figure 7, reveal that all the nuclei fall in a continuous region of negative values. In addition, as typical for covalent bonds, any Ng-H and Ng-F interaction is signed by a (3,+1) HCP. The quantitative data listed in Table 3 indicate, however, that the covalent contribution to the Ng-H and Ng-F bonds of the various HNgF is quite different. In particular, consistent with the description furnished by the ELF[14] and the AIM analysis,[26] they confirm a best description in terms of a prevailing $(H\text{-}Ng^+)(F^-)$ resonance structure, with a partially-covalent Ng-F contact. Thus, the Ng-H bond distance of any HNgF deviates from the sum of the covalent radii[56] by ca. 4%, and is definitely longer than that of the corresponding HNg^+. Consistently, compared with the HNg^+, the BD decreases by 8.8% for the H-Ar bond, and by 10.3-11.6% for the other H-Ng bonds. In any case, the predicted values range between 1.077 hartree e^{-1} (HHeF) and 0.744 hartree e^{-1} (HXeF), and are still suggestive of true covalent bonds. On the

other hand, the BDs of the Ng-F bonds are appreciably lower, and range between 0.224 hartree e^{-1} (HArF), and 0.344 hartree e^{-1} (HXeF). In addition, the percentage deviations of the Ng-F bond distances from the sum of the covalent radii[56] are, in general, appreciably higher than those predicted for the Ng-H distances. The prevailingly F^--character of the F atoms is also suggested by the position of the HCP of the Ng-F bond, which falls, particularly for HArF, HKrF, and HXeF, at a distance from F (0.96-0.98 Å) which is only slightly longer than the radius of the $H^-(\boldsymbol{r})$ region of the fluoride anion (0.950 Å, see Figure 2c). For HHeF, this distance is, however, slightly shorter (0.864 Å), and this datum mirrors a BD of the He-F bond, 0.307 hartree e^{-1}, which is higher than the corresponding values of HArF (0.224 hartree e^{-1}) and HKrF (0.280 hartree e^{-1}), and only slightly lower than the corresponding value of HXeF (0.344 hartree e^{-1}). This suggests that the He-F interaction is peculiarly tight, and this plausibly reflects the smallest size of He, which allows a deepest contact with the formal F^-. Further evidence for this "He size-effect" will be given in the forthcoming discussion.

$FNgO^-$. The $FNgO^-$ (Ng = He, Ar, Kr, Xe) are the simplest members of a somewhat special group of theoretical noble-gas anions, first highlighted by Hu and co-workers,[51] and subsequently investigated in further detail.[52,74,75] It is also of interest to note here the theoretical prediction of related neutral compounds such as $(LiF)_2(HeO)$, and other noble gas monoxides.[76,77] In general, the interaction of Ng atoms with anionic species produces weakly-bound non covalent complexes, especially for the lightest He, Ne, and Ar. Exemplary species in this regard are the $F^-(Ng)$.[78,79] The diatomic NgO are also intrinsically unstable, or only marginally stable. However, somewhat surprisingly, in the presence of F^-, the diatomic NgO, including HeO, feature a remarkably increased stability, and the ensuing $FNgO^-$ are, in general, best described by the resonance form F^-

(NgO), with a covalent Ng-O bond, and a non-covalent, or only slightly covalent F^--Ng contact. The analysis of the $H_{mol}(\boldsymbol{r})$ of the $FNgO^-$ fully confirms this description. Their bonding situation is clearly caught by inspecting subfigures a-d of Figure 8, and by examining the quantitative data listed in Table 4.

<Figure 8 and Table 4 near here, please>

We note, in particular, the spherical, or nearly-spherical, F^--like shape of the inner $H^-(\boldsymbol{r})$ regions of the F atom (whose atomic charge is invariably predicted at around -0.9 *e*), which undergoes a very weak covalent contact with HeO, KrO, and XeO (the BD amounts to only 0.0045 hartree e^{-1}, 0.053 hartree e^{-1}, and 0.123 hartree e^{-1}, respectively), and en even non-covalent contact with ArO (BD = -0.013 hartree e^{-1}). Consistently, all the HCPs fall at a distance from F of ca. 1.0 Å, which is nearly coincident with the radius of the $H^-(\boldsymbol{r})$ region of the free fluoride anion (0.950 Å). In addition, the Ng-F bond distances by far exceed the sum of the covalent radii of the two atoms.[56] On the other hand, the BD of any Ng-O bond is definitely positive, and suggests, in general, an appreciable contribution of covalency. Interestingly, the predicted values follow the order Ar-O < Kr-O < Xe-O < He-O (which mirrors a largest percentage deviation of the Ar-O bond distance from the corresponding value R_{cov}), which is different from the order of the BD of the Ng-F bonds, which increases as Ar-F < He-F < Kr-F < Xe-F. This confirms that, in the $FNgO^-$, the stabilization of the Ng-O moiety is, indeed, of electrostatic character, and is best exerted for the smallest He.

Ng-HF and NgBeO. Both the Ng-HF and the NgBeO are weakly-bound noble-gas complexes. They feature, however, peculiar differences, and it is of interest to investigate how the $H_{mol}(\boldsymbol{r})$ describes their different bonding motifs.

The Ng-HF (Ng = Ne, Ar, Kr, Xe) were recently investigated within a general study on the formation of hydrogen bonding by Ng atoms.[29,30] Thus, while Kr-HF and Xe-HF were predicted to be stable, and to feature properties typical of H-bonding contacts, Ne-HF and Ar-HF resulted even unstable when basis-set superposition error and zero-point vibrational energy corrections were included. Interestingly, the study of the $H_{mol}(\boldsymbol{r})$ actually confirms the different bonding situation of the lightest and the heaviest Ng-HF. The relevant results are given in Figure 9 and in Table 5.

<Figure 9 and Table 5 near here, please>

In general, subfigures a-e of Figure 9, showing the planar plots of the $H_{mol}(\boldsymbol{r})$ of the Ng-HF, clearly indicate their non-covalent character. The two fragments undergo a H^{+}(Ng)-H^{+}(HF) interaction, leaving their $H^{+}(\boldsymbol{r})$ regions well separated, and only little perturbed (see also Figures 1 and 5b). For He-HF, Ne-HF, and Ar-HF, this interaction is signed, in the molecular plane, by two HCPs placed symmetrically with respect to the bond axis, and belonging to the rings of degenerate HCPs signed by the arrows in subfigures f-h of Figure 9. As shown in Table 5, at these contact points, the BD progressively increases passing from He-HF (-0.233 hartree e^{-1}) to Ne-HF (-0.227 hartree e^{-1}), and Ar-HF (-0.190 hartree e^{-1}). This trend parallels the corresponding increased electronic binding energies ΔE, predicted, respectively, as 0.20 kcal mol^{-1}, 0.50 kcal mol^{-1}, and 0.86 kcal mol^{-1}. Passing to Kr-HF and Xe-HF, the contact between the two fragments is, again, topologically signed by a ring of degenerate HCPs perpendicular to the bond axis (see subfigures i and l of Figure 9), whose BD values amount to -0.129 hartree e^{-1} and -0.102 hartree e^{-1}, respectively. The most relevant finding is, however, the location of an additional (3,+1) HCP falling on the bond axis. We relate, in particular, this composite topological signature with the occurrence of a H-bond. Interestingly, at these additional

HCPs, the BD is -0.082 hartree e^{-1} for Kr-HF, and -0.033 hartree e^{-1} for Xe-HF, and both these values are higher than the BD of the corresponding ring component. If one assumes that the predicted ΔE of Kr-HF, 1.52 kcal mol^{-1}, and Xe-HF, 2.09 kcal mol^{-1}, actually reflect the tightest, on-axis contacts, a roughly linear (r^2 = 0.971) correlation does exist between the BD and the ΔE of the Ng-HF.

We note from subfigures f-l of Figure 9 that the topology of the $H_{mol}(\boldsymbol{r})$ of the Ng-HF includes the ring structures of HF (see also Figure 5e), as well as ring structures on the Ng atoms, which sign the occurrence of polarization effects by HF. Interestingly, these structures are not obtained for Ne-HF, and a lowest overall polarization occurring in this complex is also evident from subfigures a-e, which show, in particular, contour lines of the Ng atoms which deviate from the spherical shape in the irregular order Ne < He < Ar < Kr < Xe. A further example of lowest polarization of Ne was provided by the study of the NgBeO (Ng = He-Xe). These complexes are, indeed, of prototypical interest in noble-gas chemistry. They were first discovered theoretically so far by Frenking and co-workers,[22,80,81] and the heaviest ArBeO, KrBeO, and XeBeO were subsequently detected in cold matrices.[82] This stimulated a widespread interest for the ability of neutral Be-containing systems to fix the noble gases, which resulted, over the years, in the theoretical prediction of a variety of complexes,[31,83-90] and in the experimental detection of the NgBeS[11] and, quite recently, of the $NgBeCO_3$.[12]

One of the peculiar features of the neutral Ng-Be complexes, including the NgBeO, is the trend of their binding energies. Thus, while expected to progressively increase from He to Xe, the actually computed stabilities reveal a degeneracy, or nearly degeneracy, of the helium and neon congeners, the latter being, sometimes, even less stable. In particular, the most recent CCSD(T)/CBS//CCSD(T)/cc-pVTZ estimates of the

electronic binding energies ΔE of the NgBeO[12] amount to 5.1 kcal mol^{-1} (Ng = He), 4.9 kcal mol^{-1} (Ng = Ne), 11.9 kcal mol^{-1} (Ng = Ar), 13.5 kcal mol^{-1} (Ng = Kr), and 15.9 kcal mol^{-1} (Ng = Xe). The analysis of the $H_{mol}(\boldsymbol{r})$ of these species provides a reasonable explanation for this order of stability. The relevant results are shown in Figure 10 and Table 6.

<Figure 10 and Table 6 near here, please>

The plots of the $H_{mol}(\boldsymbol{r})$ of HeBeO clearly show that the He-BeO bond has two contributions. The first arises from a H^+(He)-H^+(BeO) "outer" interaction, and is signed, in the planar plot of Figure 10a, by the pair of degenerate HCPs which belong to the ring signed by the dashed arrow in Figure 10e. At these points, the BD is -0.042 hartree e^{-1}. The second contribution comes from a H^+(He)-H^+(Be) interaction, whose character is qualitatively assigned as ionic (ion-induced dipole). We note, in fact, that, according to a mechanism strictly similar to that described for NaF and NaCl (see Figure 6, a and b), the He atom overlaps nearly all of the contour lines of its $H^+(\boldsymbol{r})$ region with part of the contour lines of the $H^+(\boldsymbol{r})$ region of Be. This interaction is signed by the ring of degenerate HCPs labelled with the full arrow of Figure 10f, with a BD of -0.008 hartree e^{-1}. The $H^-(\boldsymbol{r})$ region of He is quite close to the $H^+(\boldsymbol{r})$ region of Be, and this produces the visually-caught distortion of the spherical shape of the $H^-(\boldsymbol{r})$ region of the free He (see Figure 1b for comparison). The NeBeO complex features two bond contacts qualitatively strictly similar to those predicted for HeBeO (see Figure 10g). However, while the outer component (dashed arrow of Figure 10g) has a comparable BD of -0.048 hartree e^{-1}, the inner component (full arrow) has a BD of -0.122 hartree e^{-1}, which is lower than the corresponding value predicted for HeBeO. A lower degree of interaction between Ne and Be is also caught by inspecting Figure 10b, which shows a $H^-(\boldsymbol{r})$ region

of Ne only less perturbed with respect to the spherical shape of the free Ne. Overall, our analysis suggests that HeBeO and NeBeO are non-covalent complexes, with a contribution of ionicity arising from the polarization of the Ng atom. This ion-induced dipole effect is, however, more pronounced for He, and this explains the reversed order of stability of the two species.

As for the interaction of BeO with Ar, Kr, and Xe, it is again topologically signed by two rings of degenerate HCPs (see subfigures h-l of Figure 10). The BD corresponding to the outer component (dashed arrow) is comparable with the BD of the outer components of the lighter congeners, and invariably calculated at around -0.06 hartree e^{-1}, and. On the other hand, at variance with HeBeO and NeBeO, the BDs of the inner bonding components (full arrows) are predicted to be positive, and this indicates a contribution of covalency to the interaction. The partially covalent character of the interaction of BeO with Ar, Kr, and Xe is also visually caught by inspection of subfigures c, d, and e of Figure 10, which clearly show the overlap of the $H(\boldsymbol{r})$ regions of the two fragments. It is also evident from these plots the strong polarization exerted on Ng by BeO, which results in an appreciable deformation of the spherical shape of the free Ng atoms. This suggests an appreciable contribution to the overall interaction of the ion-induced dipole component. One notes from Table 6 that the BD progressively increases from ArBeO (0.165 hartree e^{-1}) to XeBeO (0.241 hartree e^{-1}), and this parallels the progressively increased binding energies of the complexes. If one assumes that, like the Ng-HF, the ΔE of any NgBeO actually reflects the BD of the stronger bonding component, a positive correlation does again exist between the BD and the ΔE, the data being reasonably well fitted by a linear function (r^2 = 0.982), and even better interpolated by an exponential function (r^2 = 0.991).

The bonding situation of the NgBeO was so far investigated by Frenking et al.[80,81] Based on electron density analysis, they concluded that the lightest HeBeO, NeBeO, and ArBeO were bound, essentially, by charge-induced dipole interactions, even though an enhancement of the stability through HOMO-LUMO interactions could not completely be dismissed.[80] A similar description was subsequently reported[81] for the heaviest KrBeO and XeBeO, with a likely increased contribution of covalency suggested by the negative value of $H(\boldsymbol{r})$ at the BCP located on the Kr-Be and Xe-Be bond paths. In agreement with these descriptions, Boggs et al.[35] recently assigned the He-BeO, Ne-BeO, and Ar-BeO contacts as weak bonding interactions with some non-covalent (electrostatic) properties, and the Kr-BeO and Xe-BeO as weak bonding interactions with some covalent properties. These descriptions are based, essentially, on the predicted bond distances, and on the value of $H(\boldsymbol{r})$ at the BCP located on the Ng-Be bond paths. The present description of HeBeO, NeBeO, KrBeO, and XeBeO based on the analysis of their $H_{\mathrm{mol}}(\boldsymbol{r})$ is in good agreement with the previous assignments.[35,80,81] As for ArBeO, the analysis of the $H_{\mathrm{mol}}(\boldsymbol{r})$ suggests that the contribution of covalency is probably more pronounced than that estimated previously and, more interestingly, that (like KrBeO and XeBeO) this contribution actually arises from off-axis contacts between Ar and BeO. It will be, certainly, of interest to further investigate this somewhat peculiar bonding motif.

CONCLUDING REMARKS

The qualitative assignment of the interactions occurring in noble-gas compounds is a major issue in the chemistry of these elements. According to the present study, relevant

information in this regard can be obtained by a detailed analysis of the local electron energy density $H(\boldsymbol{r})$. This function, in fact, naturally partitions the space of molecular species into "covalent" and "non-covalent" regions, and allows also to recognize different types of non-covalent interactions such van der Waals, hydrogen, and ionic or partially ionic bonds. The various bonding contacts are also topologically-signed by critical points of $H(\boldsymbol{r})$, which are, in particular, characterized in terms of the bond degree (BD). This quantity was introduced previously,[54] and taken here as the ratio between the energy density calculated at the critical point of $H(\boldsymbol{r})$, and the corresponding electron density: BD = $-H(\boldsymbol{r}_c)/\rho(\boldsymbol{r}_c)$. It is positive for covalent interactions [$H(\boldsymbol{r}_c) < 0$], and negative for non-covalent ones [$H(\boldsymbol{r}_c) > 0$]. As a matter of fact, since $\rho(\boldsymbol{r}_c)$ is invariably positive, these bonding criteria simply extend the so far proposed[32,33] classification of covalent and non-covalent bonding based on the sign of the $H(\boldsymbol{r}_c)$. The BD is also positively correlated with the binding energy, but the detailed dependencies are, in general, not linear. We are currently examining other families of noble-gas compounds so to appreciate the in case effective use of $H(\boldsymbol{r})$ as a quantitative indicator of bond strength.

AUTHOR INFORMATION

Corresponding Author

*E-mail: fgrandi@unitus.it

Phone: +39-0761-357126

Notes

The authors declare no competing financial interest.

ACKNOWLEDGMENTS

The authors thank Prof. We-Ping Hu, who kindly provided some of the CCSD(T)/aug-cc-pVTZ optimized geometries, and Prof. Ruggero Caminiti (Chemistry Department, Sapienza University of Rome) for providing free computing time on NARTEN Cluster HPC Facility. The financial support of the Università della Tuscia and the Italian Ministero dell'Istruzione, dell'Università e della Ricerca (MIUR) is also gratefully acknowledged.

REFERENCES

(1) Lehmann, J.F.; Mercier, H.P.A.; Schrobilgen, G.J. The Chemistry of Krypton. *Coord. Chem. Rev.* **2002**, *233-234*, 1-39.

(2) Grochala, W. Atypical Compounds of Gases, which Have Been Called "Noble". *Chem. Soc. Rev.* **2007**, *36*, 1632-1655.

(3) Hope, E.G. Coordination Chemistry of the Noble Gases and Noble Gas Fluorides. *Coord. Chem. Rev.* **2013**, *257*, 902-909.

(4) Khriachtchev, L.; Pettersson, M.; Runeberg, N.; Lundell, J.; Räsänen, M. A Stable Argon Compound. *Nature* **2000**, *406*, 874-876.

(5) Grandinetti, F. Helium Chemistry: a Survey of the Role of Ionic Species. *Int. J. Mass Spectrom.* **2004**, *237*, 243-267, and references therein.

(6) Chałasiński, M.; Szczęśniak, M.M. Origins of Structure and Energetic of van der Waals Clusters from *ab initio* Calculations. *Chem. Rev.* **1994**, *94*, 1723-1765, and references therein.

(7) Grandinetti, F. Gas-Phase Ion Chemistry of the Noble Gases: Recent Advances and Future Perspectives. *Eur. J. Mass Spectrom.* **2011**, *17*, 423-463, and references therein.

(8) Liang, B.; Andrews, L.; Li, J.; Bursten, B.E. Noble Gas-Actinide Compounds: Evidence for the Formation of Distinct $CUO(Ar)_{4-n}(Xe)_n$ and $CUO(Ar)_{4-n}(Kr)_n$ (n = 1, 2, 3, 4) Complexes. *J. Am. Chem. Soc.* **2002**, *124*, 9016-9017.

(9) Cooke, A.S.; Gerry, M.C. XeAuF. *J. Am. Chem. Soc.* **2004**, *126*, 17000-17008.

(10) Wang, X.; Andrews, L.; Brosi, F.; Riedel, S. Matrix Infrared Spectroscopy and Quantum-Chemical Calculations for the Coinage-Metal Fluorides: Comparison of Ar-AuF, Ne-AuF, and Molecules MF_2 and MF_3. *Chem.-Eur. J.* **2013**, *19*, 1397-1409.

(11) Wang, Q.; Wang, X. Infrared Spectra of NgBeS (Ng = Ne, Ar, Kr, Xe) and BeS_2 in Noble-Gas Matrices. *J. Phys. Chem. A* **2013**, *117*, 1508-1513.

(12) Zhang, Q.; Chen, M.; Zhou, M.; Andrada, D.M.; Frenking, G. Experimental and Theoretical Studies of the Infrared Spectra and Bonding Properties of $NgBeCO_3$ and a Comparison with NgBeO (Ng = He, Ne, Ar, Kr, Xe). *J. Phys. Chem. A* **2015**, *119*, 2543-2552.

(13) Cappelletti, D.; Bartocci, A.; Grandinetti, F.; Falcinelli, S.; Belpassi, L.; Tarantelli, F.; Pirani, F. Experimental Evidence of Chemical Components in the Bonding of Helium and Neon with Neutral Molecules. *Chem.-Eur. J.* **2015**, *21*, 6234-6240.

(14) Berski, S.; Silvi, B.; Lundell, J.; Noury, S.; Latajka, Z. The Nature of Binding in HRgY Compounds (Rg = Ar, Kr, Xe; Y = F, Cl) Based on the Topological Analysis of the Electron Localisation Function (ELF), in Maruani, J.; Minot, C.; McWeeny, R.; Smeyes, Y.G.; Wilson S. (Eds.), New Trends in Quantum Systems in Chemistry and Physics, Vol. 1, Kluwer Academic Publishers, Dordrecht, 2001, 259-279.

(15) Lundell, J.; Berski, S.; Latajka, Z. Density Functional Study of the $Xe_2H_3^+$ Cation. *Chem. Phys.* **1999**, *247*, 215 -224.

(16) Berski, S.; Lundell, J.; Latajka, Z. A Density Functional Study of the Xenon Dihydride - Water Complex. *J. Mol. Struct.* **2000**, *552*, 223 - 232.

(17) Lundell, J.; Berski, S.; Latajka, Z. Dihydrogen-bonded Complexes of Xenon Dihydride with Water: Ab Initio Calculations and Topolgical Analysis of Electron Localisation Function (ELF). *Phys. Chem. Chem. Phys.* **2000**, *2*, 5521-5527.

(18) Berski, S.; Latajka, Z.; Silvi, B.; Lundell, J. Electron Localization Function Studies of the Nature of Binding in Neutral Rare-Gas Containing Hydrides: HKrCN,

HKrNC, HXeCN, HXeNC, HXeOH and HXeSH. *J. Chem. Phys.* **2001**, *114*, 4349-4358.

(19) Lundell, J.; Panek, J.; Latajka, Z. Quantum Chemical Calculations on FXeSiF. *Chem. Phys. Lett.* **2001**, *348*, 147-154.

(20) Lundell, J.; Berski, S.; Latajka, Z. Ab initio Charactrization of the Xenon Dihydride Dimer - $(HXeH)_2$ *Chem. Phys. Lett.* **2003**, *371*, 295-303.

(21) Bader, R.F.W. *Atoms in Molecules: a Quantum Theory*; Oxford University Press: Oxford, 1990.

(22) Koch, W.; Frenking, G.; Gauss, J.; Cremer, D.; Collins, J.R. Helium Chemistry: Theoretical Predictions and Experimental Challenge. *J. Am. Chem. Soc.* **1987**, *109*, 5917-5934.

(23) Frenking, G.; Koch, W.; Cremer, D.; Gauss, J.; Liebman, J.F. Helium Bonding in Singly and Doubly Charged First-Row Diatomic Cations HeX^{n+} (X = Li-Ne; n = 1, 2). *J. Phys. Chem.* **1989**, *93*, 3397-3410.

(24) Frenking, G.; Koch, W.; Cremer, D.; Gauss, J.; Liebman, J.F. Neon and Argon Bonding in First-Row Cations NeX^+ and ArX^+ (X = Li-Ne). *J. Phys. Chem.* **1989**, *93*, 3410-3418.

(25) Frenking, G.; Koch, W.; Reichel, F.; Cremer, D. Light Noble Gas Chemistry: Structures, Stabilities, and Bonding of Helium, Neon and Argon Compounds. *J. Am. Chem. Soc.* **1990**, *112*, 4240-4256.

(26) Panek, J.; Latajka, Z.; Lundell, J. DFT Calculations of HRgX (Rg = Rare gas; X = Halogen) Molecules. *Phys. Chem. Chem. Phys.* **2002**, *4*, 2504-2510.

(27) Jamshidi, Z.; Eskandari, K.; Azami, S.M. Nature of Closed- and Open-Shell Interactions between Noble Metals and Rare Gas Atoms. *Int. J. Quantum Chem.* **2013**, *113*, 1981-1991.

(28) Ghosh, A.; Manna, D.; Ghanty, T.K. Theoretical Prediction of Noble Gas Inserted Thioformyl Cations: $HNgCS^+$ (Ng = He, Ne, Ar, Kr, and Xe). *J. Phys. Chem. A* **2015**, *119*, 2233-2243.

(29) Gąszowski, D.; Ilczyszyn, M. Hydrogen Bonding to Xenon: A Comparison with Neon, Argon and Krypton Complexes. *Chem. Phys. Lett.* **2013**, *556*, 59-64.

(30) Gąszowski, D.; Ilczyszyn, M. Nature of Brønsted Acid-Noble Atom Contacts: a Reevaluation of Hydrogen Bonding Criteria. *Int. J. Quantum Chem.* **2014**, *114*, 473-480.

(31) Pan, S.; Moreno, D.; Cabellos, J.L.; Romero, J.; Reyes, A.; Merino, G.; Chattaraj, P.K. In Quest of Strong Be-Ng Bonds among the Neutral Ng-Be Complexes. *J. Phys. Chem. A* **2014**, *118*, 487-494.

(32) Cremer, D.; Kraka, E. Chemical Bonds without Bonding Electron Density - Does the Difference Electron-Density Analysis Suffice for a Description of the Chemical Bond? *Angew. Chem. Int. Ed. Engl.* **1984**, *23*, 627-628.

(33) Cremer, D.; Kraka, E. A Description of the Chemical Bond in Terms of Local Properties of Electron Density and Energy. *Croat. Chem. Acta* **1984**, *57*, 1259-1281.

(34) Ziółkowski, M.; Grabowski, S.J.; Leszczynski, J. Cooperativity in Hydrogen-Bonded Interactions: *Ab Initio* and "Atoms in Molecules" Analyses. *J. Phys. Chem. A* **2006**, *110*, 6514-6521.

(35) Zou, W.; Nori-Shargh, D.; Boggs, J. On the Covalent Character of Rare Gas Bonding Interactions: a New Kind of Weak Interaction. *J. Phys. Chem. A* **2013**, *117*, 207-212. (2013_12)

(36) Borocci, S.; Giordani, M.; Grandinetti, F. Complexes of $XeHXe^+$ with Simple Ligands: A Theoretical Investigation on $(XeHXe^+)L$ (L = N_2, CO, H_2O, NH_3). *J. Phys. Chem. A* **2015**, *119*, 2383-2392.

(37) Raghavachari, K.; Trucks, G.W.; Pople, J.A.; Head-Gordon, M. A Fifth-Order Perturbation Comparison of Electron Correlation Theories. *Chem. Phys. Lett.* **1989**, *157* 479-483.

(38) Dunning, T.H., Jr. Gaussian Basis Sets for Use in Correlated Molecular Calculations. I. The Atoms Boron through Neon and Hydrogen. *J. Chem. Phys.* **1989**, *90*, 1007-1024.

(39) Kendall, R.A.; Dunning, T.H., Jr.; Harrison, R.J. Electron Affinities of the First-Row Atoms Revisited. Systematic Basis Sets and Wave Functions. *J. Chem. Phys.* **1992**, *96*, 6796-6806.

(40) Woon, D.E.; Dunning, T.H., Jr. Gaussian Basis Sets for Use in Correlated Molecular Calculations. III. The Atoms Aluminum through Argon. *J. Chem. Phys.* **1993**, *98*, 1358-1372.

(41) Woon, D.E.; Dunning, T.H., Jr. Gaussian Basis Sets for Use in Correlated Molecular Calculations. IV. Calculation of Static Electrical Response Properties. *J. Chem. Phys.* **1994**, *100*, 2975-2989.

(42) Wilson, A.K.; Woon, D.E.; Peterson, K.A.; Dunning, T.H., Jr. Gaussian Basis Sets for Use in Correlated Molecular Calculations. IX. The Atoms Gallium through Krypton. *J. Chem. Phys.* **1999**, *110*, 7667-7677.

(43) Peterson, K.A.; Figgen, D.; Goll, E.; Stoll, H.; Dolg, M. Systematically Convergent Basis Sets with Relativistic Pseudopotentials. II. Small-Core Pseudopotentials and Correlation Consistent Basis Sets for the Post-*d* Group 16-18 Elements. *J. Chem. Phys.* **2003**, *119*, 11113-11123.

(44) Lu, T.; Chen, F. Multiwfn: A Multifunctional Wavefunction Analyzer. *J. Comput. Chem*. **2012**, *33*, 580-592.

(45) Frisch, M.J.; Trucks, G.W.; Schlegel, H.B.; Scuseria, G.E.; Robb, M.A.; Cheeseman, J.R.; Montgomery, Jr., J.A.; Vreven, T.; Kudin, K.N.; Burant, J.C. et al. *Gaussian 03*, revision D.02; Gaussian, Inc.: Wallingford, CT, 2004.

(46) Frisch, M.J.; Trucks, G.W.; Schlegel, H.B.; Scuseria, G.E.; Robb, M.A.; Cheeseman, J.R.; Scalmani, G.; Barone, V.; Mennucci, B.; Petersson, G.A. et al. *Gaussian 09*, revision D.01; Gaussian, Inc.: Wallingford, CT, 2013.

(47) NIST Chemistry WebBook, NIST Standard Reference Database Number 69 (http://webbook.nist.gov/chemistry).

(48) Giese, T.J.; York, D.M. High-Level Ab Initio Methods for Calculation of Potential Energy Surfaces of van der Waals Complexes. *Int. J. Quantum Chem.* **2004**, *98*, 388-408.

(49) Slavíček, P.; Kalus, R.; Paška, P.; Odvárková, I.; Hobza, P.; Malijevský, A. State-of-the-Art Correlated Ab Initio Potential Energy Curves for Heavy Rare Gas Dimers: Ar_2, Kr_2, and Xe_2. *J. Chem. Phys.* **2003**, *119*, 2102-2119.

(50) Borocci, S.; Bronzolino, N.; Giordani, M.; Grandinetti, F. Cationic Noble Gas Hydrides-2: A Theoretical Investigation on $HNgHNgH^+$ (Ng = Ar, Kr, Xe). *Comput. Theor. Chem.* **2011**, *964*, 318-323.

(51) Li, T.-H.; Mou, C.-H.; Chen, H.-R.; Hu, W.-P. Theoretical Prediction of Noble Gas Containing Anions $FNgO^-$ (Ng = He, Ar, and Kr). *J. Am. Chem. Soc.* **2005**, *127*, 9241-9245.

(52) Borocci, S.; Bronzolino, N.; Grandinetti, F. Noble Gas-Sulfur Anions: a Theoretical Investigation of $FNgS^-$ (Ng = He, Ar, Kr, Xe). *Chem. Phys. Lett.* **2008**, *458*, 48-53.

(53) Lai, T.-Y.; Yang, C.-Y.; Lin, H.-J.; Yang, C.-Y.; Hu, W.-P. Benchmark of Density Functional Theory Methods on the Prediction of Bond Energies and Bond Distances of Noble-Gas Containing Molecules. *J. Chem. Phys.* **2011**, *134*, 244110.

(54) Espinosa, E.; Alkorta, E.; Elguero, J.; Molins, E. From Weak to Strong Interactions: a Comprehensive Analysis of the Topological and Energetic Properties of the Electron Density Distribution Involving X-H···F-Y Systems. *J. Chem. Phys.* **2002**, *117*, 5529-5542.

(55) Kalescky, R.; Kraka , E.; Cremer, D. Identification of the Strongest Bonds in Chemistry. *J. Phys. Chem. A* **2013**, *117*, 8981-8995.

(56) Pyykkö, P.; Atsumi, M. Molecular Single-Bond Covalent Radii for Elements 1-118. *Chem. Eur. J.* **2009**, *15*, 186-197. See also: Pyykkö, P. Additive Covalent Radii for Single-, Double-, and Triple-Bonded Molecules and Tetrahedrally Bonded Crystals: A Summary. *J. Phys. Chem. A* **2015**, *119*, 2326-2337.

(57) Coxon, J.A.; Hajigeorgiou, P.G. Experimental Born-Hoppenheimer Potential for the $X^1\Sigma^+$ Ground State of HeH^+: Comparison with the Ab Initio Potential. *J. Mol. Spectrosc.* **1999**, *193*, 306-318.

(58) Ram, R.S.; Bernath, P.F.; Brault, J.W. Fourier Transform Emission Spectroscopy of Protonated Neon (NeH^+). *J. Mol. Spectrosc.* **1985**, *113*, 451-457.

(59) Laughlin, K.B.; Blake, G.A.; Cohen, R.C.; Hovde, D.C.; Saykally, R.J. Determination of the Dipole Moment of ArH^+ from the Rotational Zeeman Effect by Tunable Far Infrared Laser Spectroscopy. *Phys. Rev. Lett.* **1987**, *58*, 996-999.

(60) Linnartz, H.; Havenith. M.; Zwart, E.; Meerts, W.L.; ter Meulen, J.J. Determination of the Electric Dipole Moment of KrH^+. *J. Mol. Spectrosc.* **1997**, *153*, 710-717.

(61) Rogers, S.A.; Brazier, C.R.; Bernath, P.F. The Infrared Spectrum of XeH^+. *J. Chem. Phys.* **1987**, *87*, 159-162.

(62) Lundell, J. Density Functional Approach on Ground State RgH^+ and $RgHRg^+$ (Rg = Ar, Kr, Xe) Ions. *J. Mol. Struct.* **1995**, *355*, 291-297.

(63) Barlow, M.J.; Swinyard, B.M.; Owen, P.J.; Cernicharo, J.; Gomez, H.L.; Ivison, R.J.; Krause, O.; Lim, T.L.; Matsuura, M.; Miller, S. et al. Detection of a Noble Gas Molecular Ion, $^{36}ArH^+$, in the Crab Nebula. *Science* **2013**, *342*, 1343-1345.

(64) Schilke, P.; Neufeld, D.A.; Müller, H.S.P.; Comito, C.; Bergin, E.A.; Lis, D.C.; Gerin, M.; Black, J.H.; Wolfire, M.; Indriolo N. et al. Ubiquitous Argonium (ArH^+) in the Diffuse Interstellar Medium: A Molecular Tracer of almost Purely Atomic Gas. *Astron. Astrophys*. **2014**, *566*, A29.

(65) Roueff, E.; Alekseyev, A.B.; Bourlot, J.L. Photodissociation of interstellar ArH^+. *Astron. Astrophys*. **2014**, *566*, A30.

(66) Pettersson, M.; Lundell, J.; Räsänen, M. New Rare-Gas-Containing Neutral Molecules. *Eur. J. Inorg. Chem.* **1999**, 729-737.

(67) Gerber, R.B. Formation of Novel Rare-Gas Molecules in Low-Temperature Matrices. *Annu. Rev. Phys. Chem.* **2004**, *55*, 55-78.

(68) Khriachtchev, L.; Räsänen, M.; Gerber, R.B. Noble-Gas Hydrides: New Chemistry at Low Temperatures. *Acc. Chem. Res.* **2009**, *42*, 183-191.

(69) Grochala, W.; Khriachtchev, L.; Räsänen, M. Noble-Gas Chemistry. in *Physics and Chemistry at Low Temperatures*; Khriachtchev, L., Ed.; CRC Press: 2011; pp 419-446.

(70) Pettersson, M.; L. Khriachtchev, L.; A. Lignell, A.; M. Räsänen, M.; Z. Bihary, Z.; Gerber, R.B. HKrF in Solid Krypton. *J. Chem. Phys.* **2002**, *116*, 2508-2515.

(71) Huang, Z.G.; Xie, D.Q.; Zhu, H.H. Theoretical Studies on the Potential Energy Surfaces and Vibrational Energy Levels of HXeF and HXeCl. *Sci. China Ser. B* **2007**, *50*, 7-10.

(72) Wong, M.H. Prediction of a Metastable Helium Compound: HHeF. *J. Am. Chem. Soc.* **2000**, *122*, 6289-6290.

(73) Takayanagi, T.; Wada, A. Theoretical Prediction of the Lifetime of the Metastable Helium Compound: HHeF. *Chem. Phys. Lett.* **2002**, *352*, 91-98.

(74) Liu, Y.-L.; Chang, Y.-H.; Li, T.-H.; Chen, H.R.; Hu, W.-P. Theoretical Study on the Noble-Gas Anions $F^-(NgO)_n$ (Ng = He, Ar, and Kr). *Chem. Phys. Lett.* **2007**, *439*, 14-17.

(75) Li, Y.; Ai, H.; Qi, Z.; He, W.; Zhang, L., Stability Analysis of the Neutral Noble Gas Molecule FNgX and their Anions $FNgX^-$ (Ng = He, Ar, Kr; X = O, S). *Int. J. Quantum Chem.* **2009**, *109*, 782-789.

(76) Grochala, W. Metastable He-O Bond inside a Ferroelectric Molecular Cavity: $(HeO)(LiF)_2$. *Phys. Chem. Chem. Phys.* **2012**, *14*, 14860-14868.

(77) Szarek, P.; Grochala, W. Noble Gas Monoxides Stabilized in a Dipolar Cavity: A Theoretical Study. *J. Phys. Chem. A* **2015**, *119*, 2483-2489.

(78) Gray, B.R.; Wright, T.G.; Wood, E.L.; Viehland, L.A. Accurate Potential Energy Curves for F^--Rg (Rg = He-Rn): Spectroscopy and Transport Coefficients. *Phys. Chem. Chem. Phys.* **2006**, *8*, 4752-4757.

(79) Wada, A.; Kikkawa, A.; Sugiyama, T.; Hiraoka, K. Thermochemical Stabilities of the Gas-Phase Cluster Ions of Halide Ions with Rare Gas Atoms. *Int. J. Mass Spectrom.* **2007**, *267*, 284-287.

(80) Frenking, G.; Koch, W.; Gauss, J.; Cremer, D. Stabilities and Nature of the Attractive Interactions in HeBeO, NeBeO, and ArBeO and a Comparison with Analogues NGLiF, NGBN, and NGLiH (NG = He, Ar). A Theoretical Investigation. *J. Am. Chem. Soc.* **1988**, *110*, 8007-8016.

(81) Veldkamp, A.; Frenking, G. Structures and Bond Energies of the Noble Gas Complexes NgBeO (Ng = Ar, Kr, Xe). *Chem. Phys. Lett.* **1994**, *226*, 11-16.

(82) Thompson, C.A.; Andrews, L. Noble Gas Complexes with BeO: Infrared Spectra of NG-BeO (NG = Ar, Kr, Xe). *J. Am. Chem. Soc.* **1994**, *116*, 423-424.

(83) Antoniotti, P.; Bronzolino, N.; Grandinetti, F. Stable Compounds of the Lightest Noble Gases: a Computational Investigation on RNBeNg (Ng = He, Ne, Ar). *J. Phys. Chem. A* **2003**, *107*, 2974-2980.

(84) Borocci, S.; Bronzolino, N.; Grandinetti, F. From OBeHe to $H_3BOBeHe$: Enhancing the Stability of a Neutral Helium Compound. *Chem. Phys. Lett.* **2005**, *406*, 179-183.

(85) Borocci, S.; Bronzolino, N.; Grandinetti, F. Neutral Helium Compounds: Theoretical Evidence for a Large Class of Polynuclear Complexes. *Chem. Eur. J.* **2006**, *12*, 5033-5042.

(86) Takayanagi, T.; Motegi, H.; Taketsugu, Y.; Taketsugu, T. Accurate Ab Initio Electronic Structure Calculations of the Stable Helium Complex HeBeO. *Chem. Phys. Lett.* **2008**, *454*, 1-6.

(87) Motegi, H.; Kakizaki, A.; Takayanagi, T.; Taketsugu, Y.; Taketsugu, T.; Shiga, M. Path-Integral Molecular Dynamics Simulations of BeO Embedded in Helium Clusters: Formation of the Stable HeBeO Complex. *Chem. Phys.* **2008**, *354*, 38-43.

(88) Kobayashi, T.; Kohno, Y.; Takayanagi, T.; Seki, K.; Ueda, K. Rare Gas Bond Property of Rg-Be_2O_2 and Rg-Be_2O_2-Rg (Rg = He, Ne, Ar, Kr and Xe) as a Comparison with Rg-BeO. *Comput. Theor. Chem.* **2012**, *991*, 48-55.

(89) Pan, S.; Jalife, S.; Kumar, R.M.; Subramanian, V.; Merino, G.; Chattaraj, P.K. Structure and Stability of $(NG)_nCN_3Be_3^+$ Clusters and Comparison with $(NG)BeY^{0/+}$. *ChemPhysChem* **2013**, *14*, 2511-2517.

(90) Hapka, M.; Klos, J.; Korona, T.; Chałasiński, G. Theoretical Studies of Potential Energy Surface and Bound States of the Strongly Bound He(^{1}S)-BeO($^1\Sigma^+$) Complex. *J. Phys. Chem. A* **2013**, *117*, 6657-6663.

Table 1. Properties of the Central Non-Covalent HCPs of the Ng_2 (see also Figure 4)

Ng_2	R^a	$(\hat{r},s)^b$	$H(\boldsymbol{r}_c)^c$	$\rho(\boldsymbol{r}_c)^d$	$-H(\boldsymbol{r}_c)/\rho(\boldsymbol{r}_c)$	ΔE^e
He_2	3.017	(3,-1)	0.00037	0.0008	-0.463	0.02
Ne_2	3.109	(3,-1)	0.00068	0.0023	-0.296	0.11
		(3,-3)	0.00068	0.0022	-0.309	
Ar_2	3.815	(3,-1)	0.00069	0.0027	-0.256	0.27
Kr_2	4.019	(3,-1)	0.00080	0.0032	-0.250	0.55
Xe_2	4.347	(3,-1)	0.00050	0.0035	-0.180	0.82

[a]CCSD(T)/aug-cc-pVTZ bond distance (Å). [b]Rank and signature of the HCP. [c]Energy density (hartree a_0^{-3}) at the HCP. [d]Electron density ($e\ a_0^{-3}$) at the HCP. [e]CCSD(T)/aug-cc-pVTZ electronic binding energy (kcal mol^{-1}).

Table 2. Properties of the Covalent (3,+1) HCPs of H_2, HF, and F_2 (see also Figure 5)

	R^a	$H(\mathbf{r}_c)^b$	$\rho(\mathbf{r}_c)^c$	$-H(\mathbf{r}_c)/\rho(\mathbf{r}_c)$	ΔE^d
H_2	0.743	-0.30794	0.2678	1.150	104.2
HF	0.921	-0.53452	0.4434	1.206	135.0
F_2	1.418	-0.17945	0.2797	0.642	38.0

[a]CCSD(T)/aug-cc-pVTZ bond distance (Å). [b]Energy density (hartree a_0^{-3}) at the HCP. [c]Electron density ($e\ a_0^{-3}$) at the HCP. [d]Experimental homolytic bond dissociation energy (kcal mol^{-1}) taken from Ref. 47.

Table 3. Properties of the Covalent (3,+1) HCPs of HNg^+ and HNgF (see also Figure 7)

	Ng-H						
	R^a	$R_{cov}{}^b$	r(H)^c	r(Ng)^c	$H(\mathbf{r}_c)^d$	$\rho(\mathbf{r}_c)^e$	$-H(\mathbf{r}_c)/\rho(\mathbf{r}_c)^f$
HHe^+	0.776 (-0.5%)	0.78	0.287	0.489	-0.33082	0.2716	1.218
HHeF	0.811 (4.5%)	0.78	0.322	0.489	-0.30891	0.2867	1.077 (11.6%)
HNe^+	0.992 (0.2%)	0.99	0.319	0.673	-0.33038	0.3085	1.071
HAr^+	1.282 (0.2%)	1.28	0.379	0.903	-0.23925	0.2450	0.977
HArF	1.329 (3.7%)	1.28	0.410	0.919	-0.20446	0.2295	0.891 (8.8%)
HKr^+	1.413 (-5.4%)	1.49	0.418	0.995	-0.20224	0.2128	0.950
HKrF	1.477 (4.5%)	1.49	0.470	1.007	-0.16372	0.1921	0.852 (10.3%)
HXe^+	1.595 (-2.2%)	1.63	0.562	1.033	-0.14544	0.1731	0.840
HXeF	1.663 (4.3%)	1.63	0.615	1.048	-0.11288	0.1518	0.744 (11.4%)
	Ng-F						
	R^a	$R_{cov}{}^b$	r(F)^c	r(Ng)^c	$H(\mathbf{r}_c)^d$	$\rho(\mathbf{r}_c)^e$	$-H(\mathbf{r}_c)/\rho(\mathbf{r}_c)$
HHeF	1.415 (22.3%)	1.10	0.864	0.551	-0.04355	0.1419	0.307
HArF	1.979 (19.2%)	1.60	0.966	1.013	-0.02184	0.0976	0.224
HKrF	2.042 (11.4%)	1.81	0.963	1.079	-0.02738	0.0978	0.280
HXeF	2.116 (7.8%)	1.95	0.977	1.139	-0.03306	0.0961	0.344

[a]CCSD(T)/aug-cc-pVTZ bond distance (Å). The value in parenthesis is the percentage deviation from R_{cov}. [b]Sum of the covalent radii (Å) taken from Ref. 56. [c]Distance (Å) of the HCP from the atom in parenthesis. [d]Energy density (hartree a_0^{-3}) at the HCP. [e]Electron density ($e\ a_0^{-3}$) at the HCP. [f]The value in parenthesis is the percentage decrease with respect to the value of the corresponding HNg^+.

Table 4. Properties of the (3,+1) Bonding HCPs of $FNgO^-$ (see also Figure 8)

	Ng-F						
	R^a	$R_{cov}{}^b$	r(F)^c	r(Ng)^c	$H(\boldsymbol{r}_c)^d$	$\rho(\boldsymbol{r}_c)^e$	$-H(\boldsymbol{r}_c)/\rho(\boldsymbol{r}_c)$
$FHeO^-$	1.626 (32.3%)	1.10	1.011	0.615	-0.00035	0.0773	0.0045
$FArO^-$	2.241 (28.6%)	1.60	1.065	1.176	0.00075	0.0507	-0.013
$FKrO^-$	2.259 (19.9%)	1.81	1.044	1.215	-0.00308	0.0580	0.053
$FXeO^-$	2.321 (16.0%)	1.95	1.035	1.286	-0.00760	0.0616	0.123
	Ng-O						
	R^a	$R_{cov}{}^b$	r(O)^c	r(Ng)^c	$H(\boldsymbol{r}_c)^d$	$\rho(\boldsymbol{r}_c)^e$	$-H(\boldsymbol{r}_c)/\rho(\boldsymbol{r}_c)$
$FHeO^-$	1.110 (1.8%)	1.09	0.622	0.488	-0.26205	0.3088	0.849
$FArO^-$	1.781 (10.7%)	1.59	0.781	1.000	-0.07973	0.1677	0.475
$FKrO^-$	1.854 (2.9%)	1.80	0.792	1.062	-0.09184	0.1709	0.537
$FXeO^-$	1.967 (1.4%)	1.94	0.841	1.126	-0.09356	0.1579	0.593

[a]CCSD(T)/aug-cc-pVTZ bond distance (Å). The value in parenthesis is the percentage deviation from R_{cov}. [b]Sum of the covalent radii (Å) taken from Ref. 56. [c]Distance (Å) of the HCP from the atom in parenthesis. [d]Energy density (hartree a_0^{-3}) at the HCP. [e]Electron density ($e\ a_0^{-3}$) at the HCP.

Table 5. Properties of the Bonding HCPs of Ng-HF (see also Figure 9)

	Ng-H					
	R^a	$(\hat{r},s)^b$	$H(\boldsymbol{r}_c)^c$	$\rho(\boldsymbol{r}_c)^d$	$-H(\boldsymbol{r}_c)/\rho(\boldsymbol{r}_c)$	ΔE^e
He-HF	2.226_5	ring	0.00119	0.0051	-0.233	0.20
Ne-HF	2.234	ring	0.00136	0.0060	-0.227	0.50
Ar-HF	2.506	ring	0.00131	0.0069	-0.190	0.86
Kr-HF	2.535	ring	0.00090	0.0070	-0.129	1.52
		(3,+1)	0.00095	0.0116	-0.082	
Xe-HF	2.677	ring	0.00052	0.0051	-0.102	2.09
		(3,+1)	0.00040	0.0123	-0.033	
	H-F					
	R^a	$(\hat{r},s)^b$	$H(\boldsymbol{r}_c)^c$	$\rho(\boldsymbol{r}_c)^d$	$-H(\boldsymbol{r}_c)/\rho(\boldsymbol{r}_c)$	
He-HF	0.921	(3,+1)	-0.53424	0.4433	1.205	
Ne-HF	0.921	(3,+1)	-0.53449	0.4434	1.205	
Ar-HF	0.922	(3,+1)	-0.53143	0.4420	1.202	
Kr-HF	0.923	(3,+1)	-0.52856	0.4408	1.199	
Xe-HF	0.924	(3,+1)	-0.52534	0.4394	1.196	

[a]CCSD(T)/aug-cc-pVTZ bond distance (Å). [b]Rank and signature of the HCP. [c]Energy density (hartree a_0^{-3}) at the HCP. [d]Electron density ($e\ a_0^{-3}$) at the HCP. [e]CCSD(T)/aug-cc-pVTZ electronic binding energy (kcal mol^{-1}).

Table 6. Properties of the Bonding Ring HCPs of NgBeO (see also Figure 10)

	R^a	$R_{cov}{}^b$	$H(\boldsymbol{r}_c)^c$	$\rho(\boldsymbol{r}_c)^d$	$-H(\boldsymbol{r}_c)/\rho(\boldsymbol{r}_c)$	ΔE^e
HeBeO	1.524 (2.9%)	1.48	0.00010	0.0122	-0.008	5.1
			0.00008	0.0019	-0.042	
NeBeO	1.799 (6.1%)	1.69	0.00426	0.0350	-0.122	4.9
			0.00010	0.0021	-0.048	
ArBeO	2.073 (4.5%)	1.98	-0.00214	0.0130	0.165	11.9
			0.00015	0.0025	-0.060	
KrBeO	2.201 (0.5%)	2.19	-0.00276	0.0132	0.209	13.5
			0.00016	0.0027	-0.059	
XeBeO	2.370 (1.7%)	2.33	-0.00340	0.0141	0.241	15.9
			0.00017	0.0027	-0.063	

[a]CCSD(T)/aug-cc-pVTZ Ng-Be bond distance (Å). The value in parenthesis is the percentage deviation from R_{cov}. [b]Sum of the covalent radii (Å) taken from Ref. 56. [c]Energy density (hartree a_0^{-3}) at the HCP. [d]Electron density ($e\ a_0^{-3}$) at the HCP. [e]CCSD(T)/CBS//CCSD(T)/cc-pVTZ electronic binding energy (kcal mol^{-1}) taken from Ref. 12.

Captions for Figures

Figure 1. $H(\boldsymbol{r})$ of H, He, Ne, Ar, Kr, and Xe plotted in planes containing the nuclei. Solid and dashed lines (blue and brown in the on-line version) correspond, respectively, to positive and negative values.

Figure 2. $H(\boldsymbol{r})$ of F, F^-, Cl^-, Li^+, and Na^+ plotted in planes containing the nuclei. Solid and dashed lines (blue and brown in the on-line version) correspond, respectively, to positive and negative values.

Figure 3. Radial dependence of the $H(\boldsymbol{r})$ of He and F^- in the outer region of positive values. R is the distance from the outer limit [$H(\boldsymbol{r}) = 0$] of the region of negative values.

Figure 4. Subfigures a-e: $H_{mol}(\boldsymbol{r})$ of Ng_2 (Ng = He-Xe) plotted in the main molecular plane. Solid and dashed lines (blue and brown in the on-line version) correspond, respectively, to positive and negative values. The dots sign the non-covalent (3,-1) HCPs. Subfigures f-l: 3D view of the HCPs located from the topological analysis of the $H_{mol}(\boldsymbol{r})$ (the critical points near the nuclei are not shown). The arrows sign the non-covalent (3,-1) HCPs.

Figure 5. Subfigures a-c: $H_{mol}(\boldsymbol{r})$ of H_2, HF, and F_2 plotted in the main molecular plane. Solid and dashed lines (blue and brown in the on-line version) correspond, respectively, to positive and negative values. The dots sign the covalent (3,+1) HCPs. Subfigures d-f:

3D view of the HCPs located from the topological analysis of the $H_{mol}(\boldsymbol{r})$ (the critical points near the nuclei are not shown). The arrows sign the covalent (3,+1) HCPs.

Figure 6. $H_{mol}(\boldsymbol{r})$ of NaF, NaCl, and BeO plotted in the main molecular plane. Solid and dashed lines (blue and brown in the on-line version) correspond, respectively, to positive and negative values. For NaF and NaCl, the dots sign pairs of non-covalent HCPs lying in the plane and belonging to ring structures. For BeO, the dot signs the covalent (3,-1) HCP.

Figure 7. $H_{mol}(\boldsymbol{r})$ of HNg^+ (Ng = He-Xe) (subfigures a-e) and HNgF (Ng = He, Ar-Xe) (subfigures f-i) plotted in the main molecular plane. Solid and dashed lines (blue and brown in the on-line version) correspond, respectively, to positive and negative values. The dots sign the covalent (3,+1) HCPs.

Figure 8. $H_{mol}(\boldsymbol{r})$ of $FNgO^-$ plotted in the main molecular plane. Solid and dashed lines (blue and brown in the on-line version) correspond, respectively, to positive and negative values. The dots sign the (3,+1) HCPs.

Figure 9. Subfigures a-e: $H_{mol}(\boldsymbol{r})$ of Ng-HF (Ng = He-Xe) plotted in the main molecular plane. Solid and dashed lines (blue and brown in the on-line version) correspond, respectively, to positive and negative values. Subfigures f-l: 3D view of the HCPs located from the topological analysis of the $H_{mol}(\boldsymbol{r})$ (the critical points near the nuclei are not shown). The off-axis bonding HCPs signed by circles in subfigures a-e belong to

the rings signed by arrows in subfigures f-l. For Kr-HF and Xe-HF, the on-axis bonding HCPs are also signed.

Figure 10. Subfigures a-e: $H_{mol}(\boldsymbol{r})$ of NgBeO (Ng = He-Xe) plotted in the main molecular plane. Solid and dashed lines (blue and brown in the on-line version) correspond, respectively, to positive and negative values. Subfigures f-l: 3D view of the HCPs located from the topological analysis of the $H_{mol}(\boldsymbol{r})$ (the critical points near the nuclei are not shown). The off-axis bonding HCPs signed by dots in subfigures a-e belong to the rings signed by arrows in subfigures f-l.

Figure 1

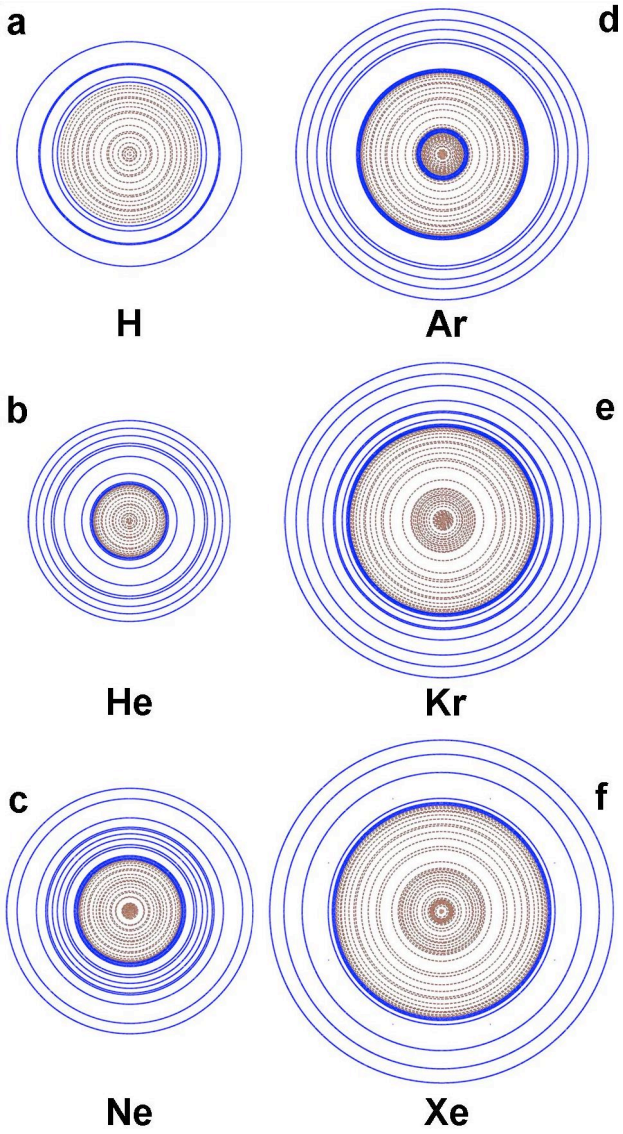

Figure 2

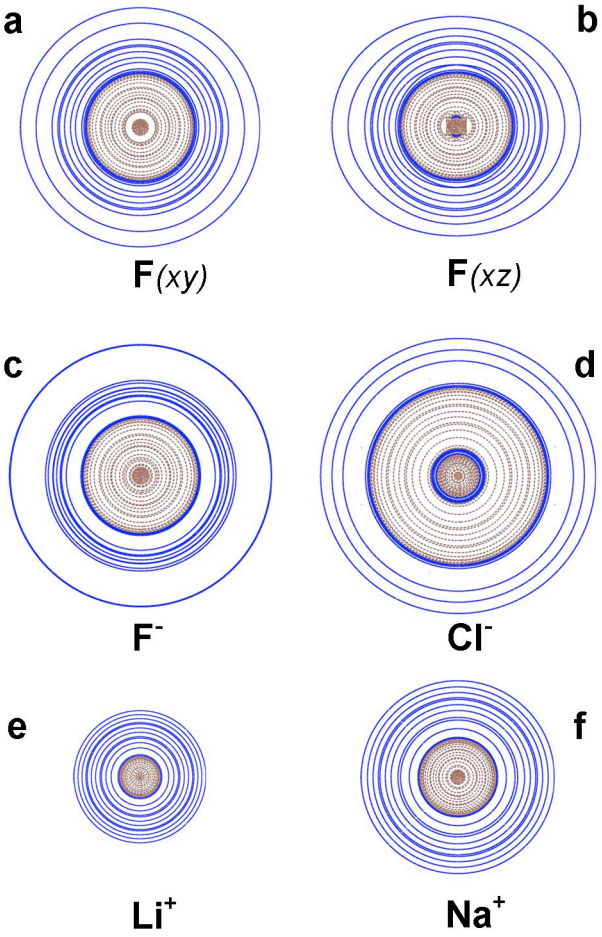

Figure 3

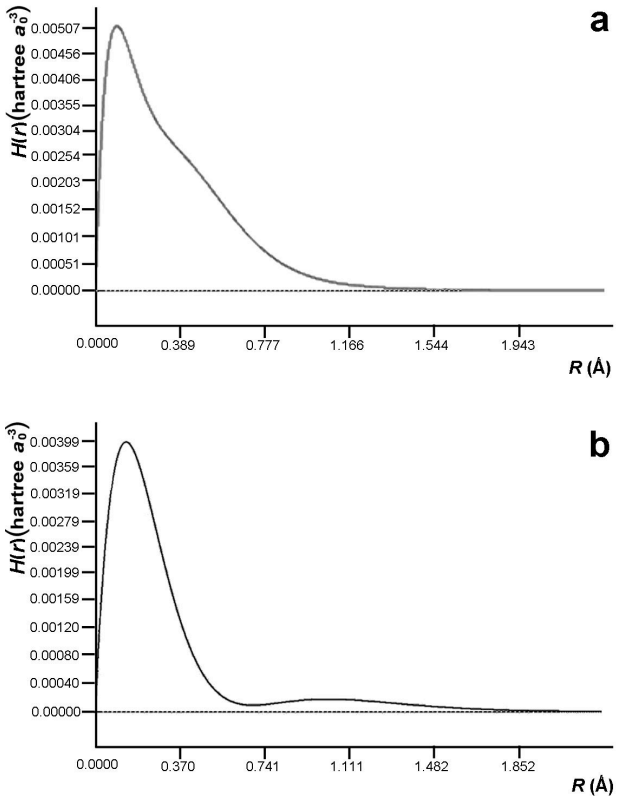
a
H(r)(hartree a0-3)
0.00507
0.00456
0.00406
0.00355
0.00304
0.00254
0.00203
0.00152
0.00101
0.00051
0.00000
0.0000
0.389
0.777
1.166
1.544
1.943
R (Å)
b
H(r)(hartree a0-3)
0.00399
0.00359
0.00319
0.00279
0.00239
0.00199
0.00159
0.00120
0.00080
0.00040
0.00000
0.0000
0.370
0.741
1.111
1.482
1.852
R (Å)

Figure 4

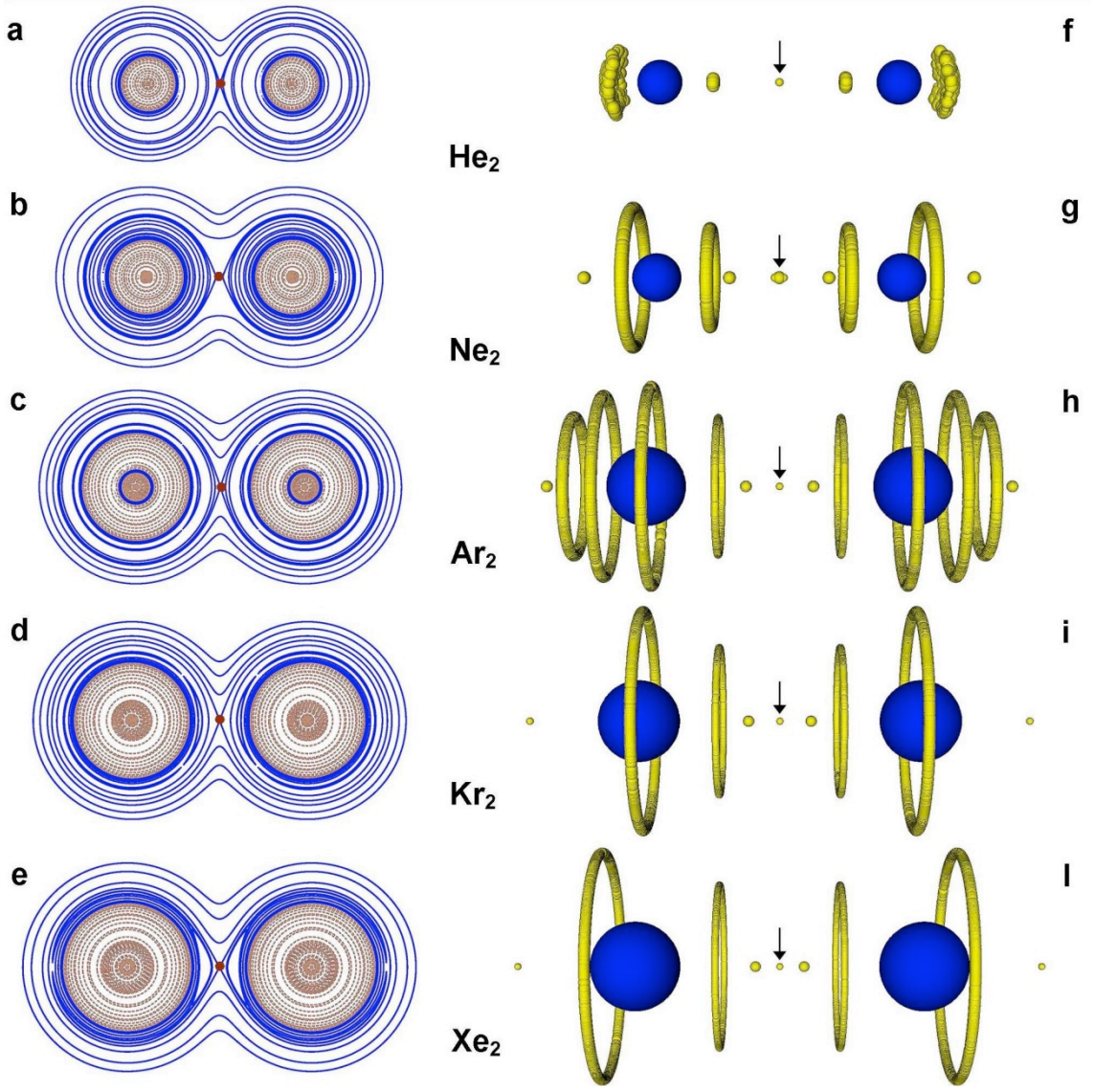

Figure 5

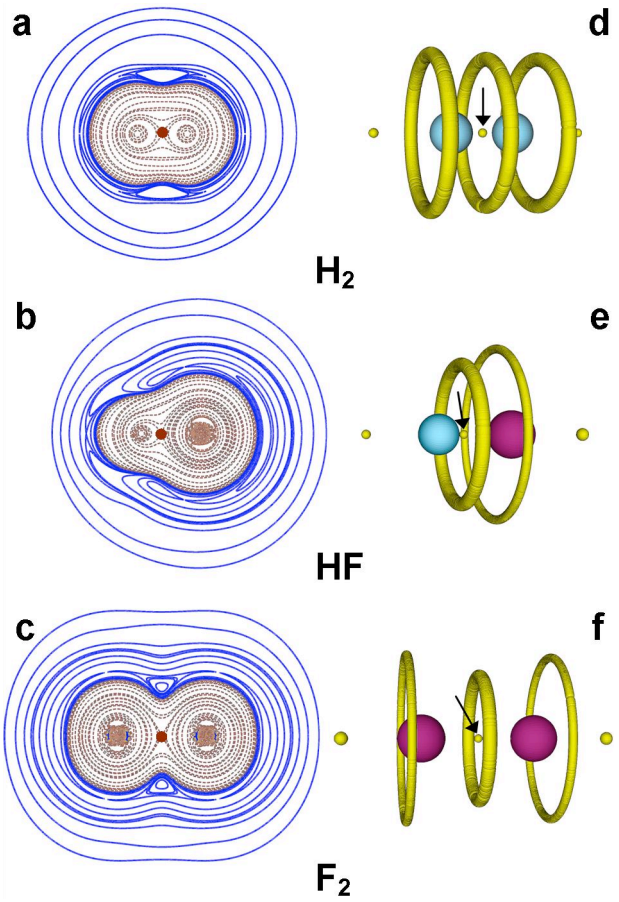

Figure 6

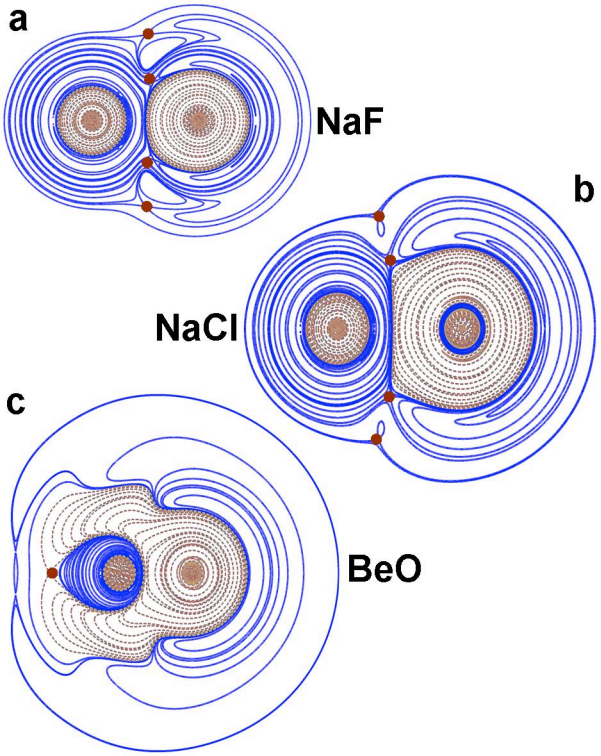

Figure 7

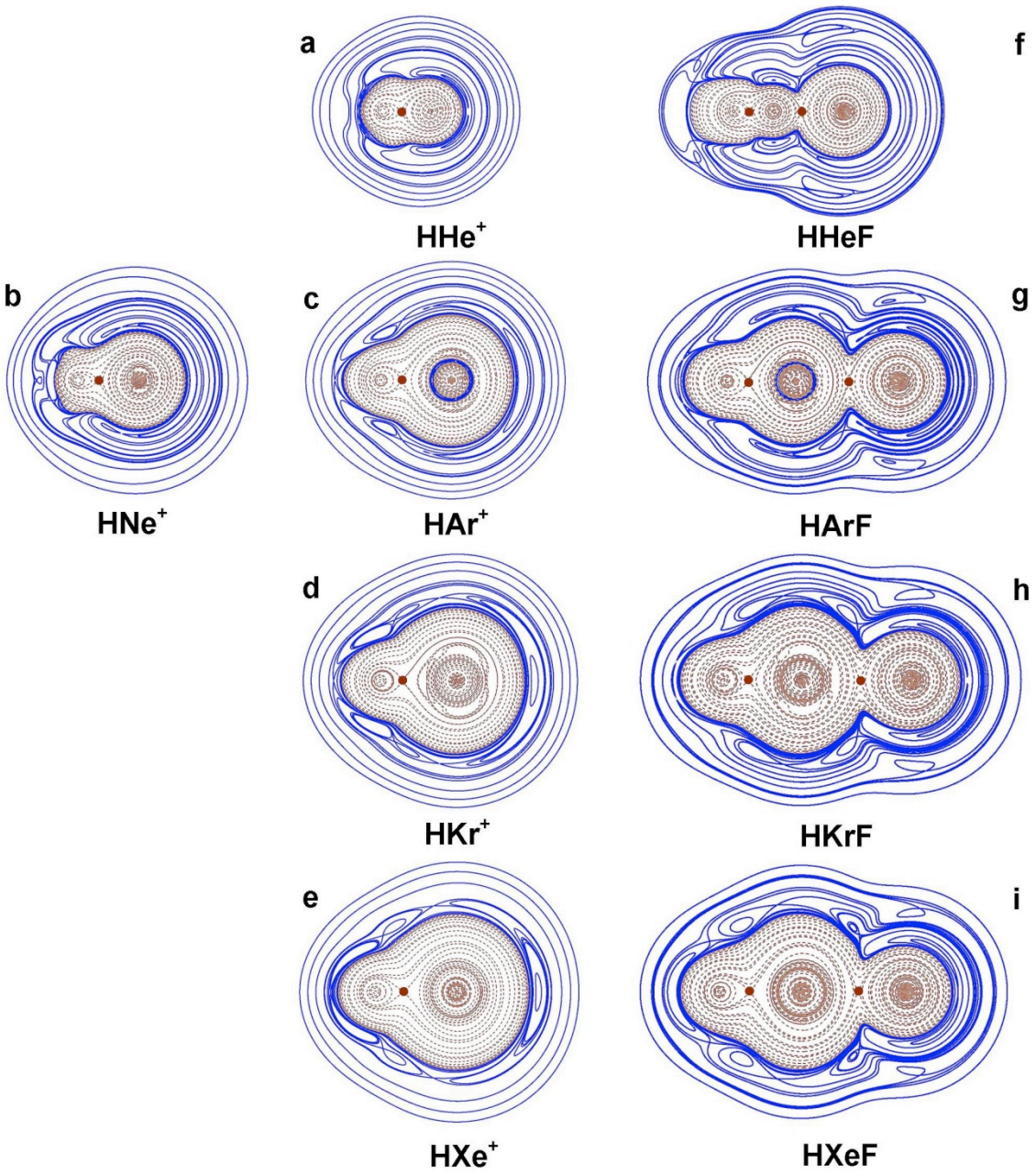

Figure 8

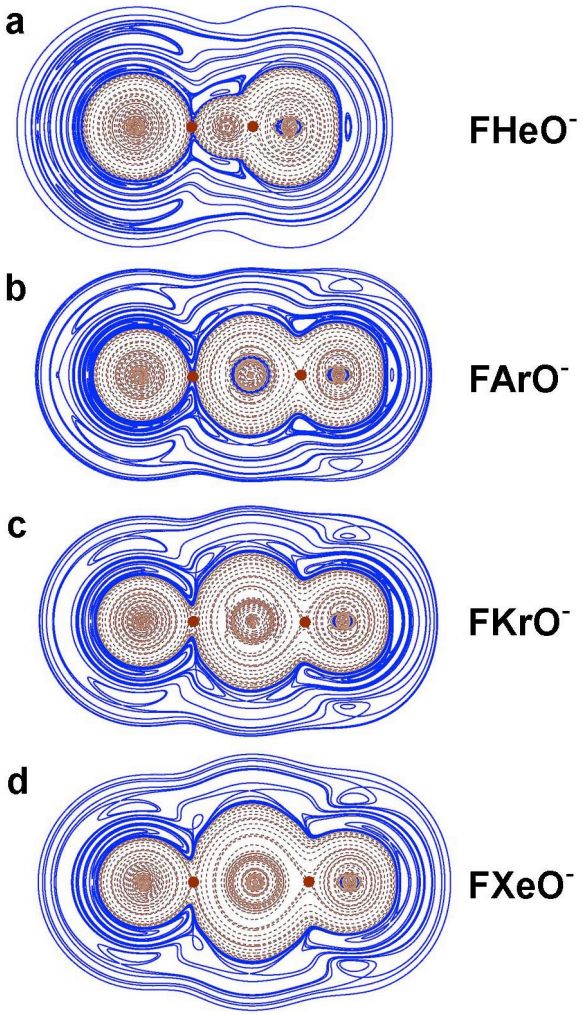

Figure 9

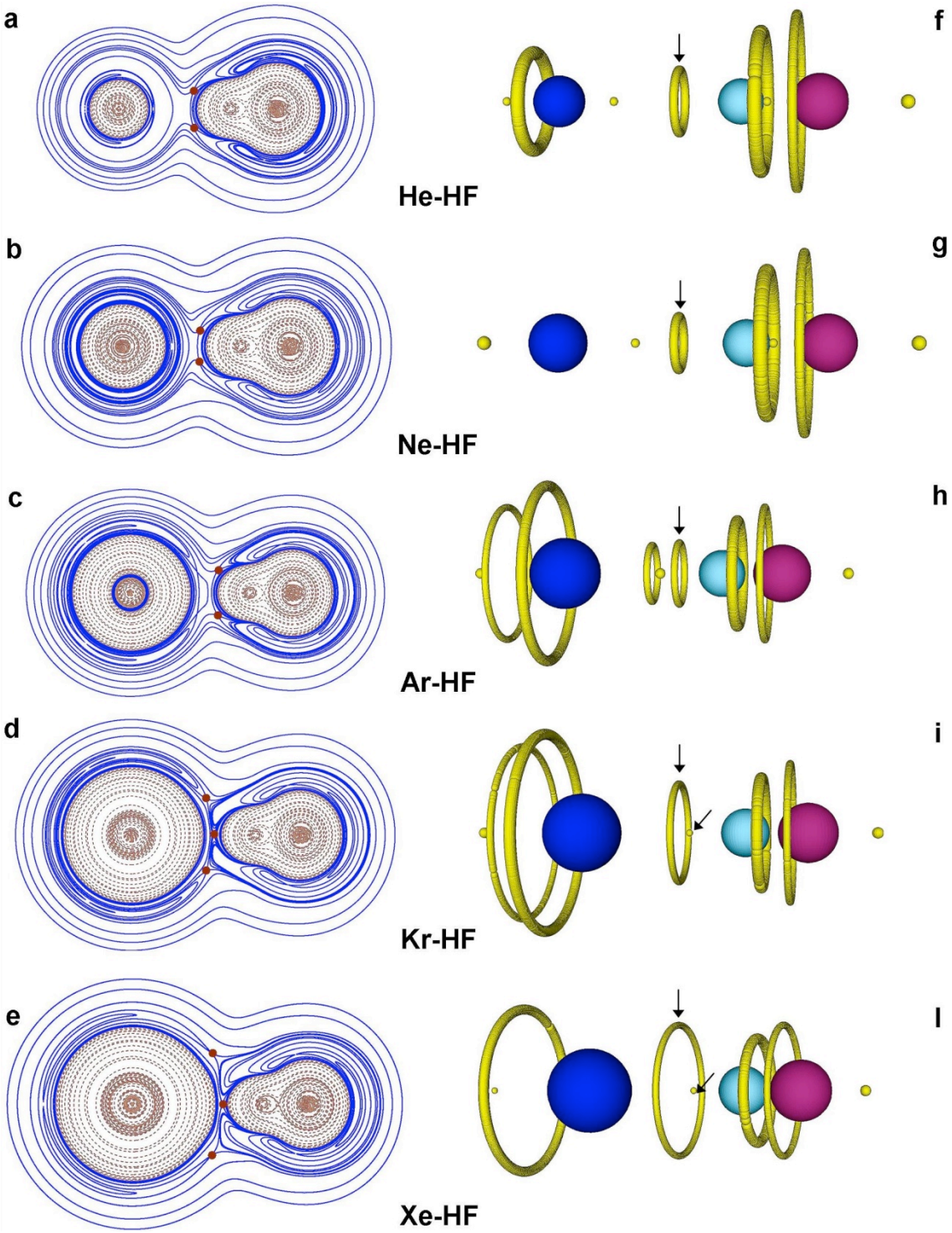

Figure 10

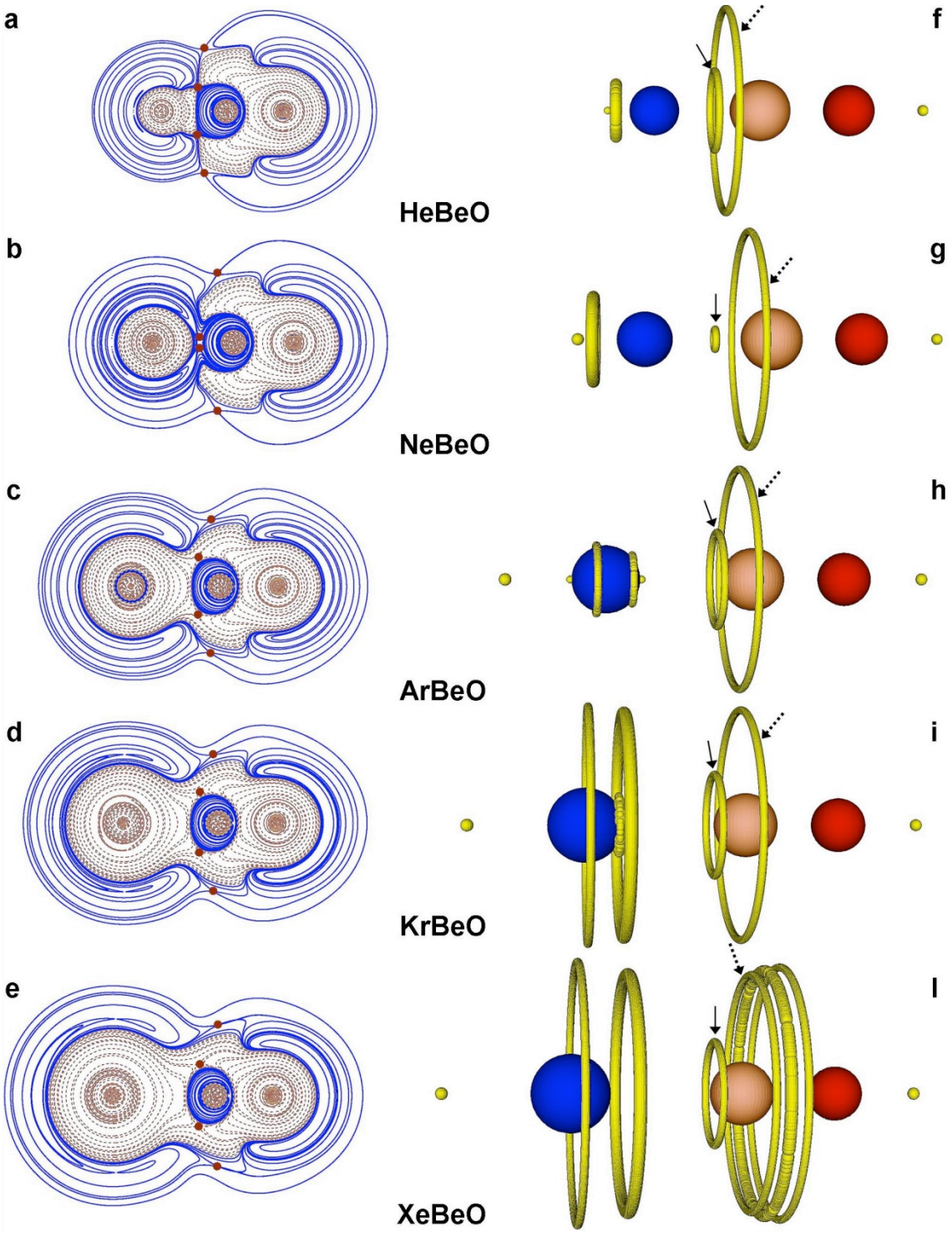

TOC